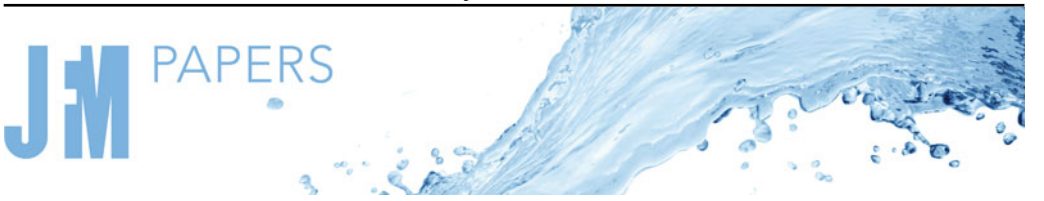
J. Fluid Mech. (2026), *vol.* 1031, A15, doi:10.1017/jfm.2026.11292



Transient dispersion in oscillatory flows: auxiliary-time extension method for concentration moments

Weiquan Jiang[1] and **Guoqian Chen**[2,1]

[1]Key Laboratory of River Basin Digital Twinning of Ministry of Water Resources, National Observation and Research Station of Coastal Ecological Environments in Macao, Macau Environmental Research Institute, Macau University of Science and Technology, Macao SAR 999078, PR China

[2]Laboratory of Systems Ecology and Sustainability Science, Department of Mechanics, Peking University, Beijing 100871, PR China

Corresponding author: Guoqian Chen, gqchen@pku.edu.cn

(Received 11 March 2025; revised 2 December 2025; accepted 1 February 2026)

The dispersion phenomenon of mass and heat transport in oscillatory flows has wide applications in environmental, physiological and microfluidic flows. The method of concentration moments is a powerful theoretical framework for analysing transport characteristics and is well developed for steady flows: general solution expressions of moments have been profoundly derived by Barton (*J. Fluid Mech.* 126, 1983, 205–218). However, it was thought that these expressions could not be directly applied to unsteady flows. Prior studies needed to re-solve the governing equations of moments from scratch, encountering the complication induced by the time-periodic velocity, leaving higher-order statistics like skewness and kurtosis analytically intractable except for specific cases. This work proposes a novel approach based on a two-time-variable extension to tackle these challenges. By introducing an auxiliary time variable, referred to as oscillation time to characterise the inherent oscillation in the dispersion due to the oscillating flow, the transport problem is extended to a two-time-variable system with a 'steady' flow term. This enables the direct use of Barton's expressions and thus avoids the prior complication. This approach not only offers an intuitive physical perspective for the influence of the velocity oscillation, but also clarifies the solution structure of concentration moments. As a preliminary verification, we examine the transport problem in an oscillatory Couette flow. The analytical solution agrees well with the numerical result by Brownian dynamics simulations. The effects of the point-source release and the phase shift of velocity on the transport characteristics are investigated. By extending the classic steady-flow solution to the time-dependent flows, this work provides a versatile framework for transient dispersion analysis, enhancing predictions in oscillatory transport problems.

© The Author(s), 2026. Published by Cambridge University Press.

https://doi.org/10.1017/jfm.2026.11292 Published online by Cambridge University Press

Key words: dispersion, mass transport

1. Introduction

The dispersion phenomenon of mass and heat transport in oscillatory flows has a wide range of applications, from environmental flows in estuaries (Holley, Harleman & Fischer 1970; Fischer 1972), wetlands (Zeng *et al.* 2012; Guan *et al.* 2021) and oceans (Yasuda 1984; Zeng *et al.* 2025*b*), to pulsating flows in physiological systems (Grotberg, Sheth & Mockros 1990; Jiang & Grotberg 1993; Grotberg & Jensen 2004; Lawrence *et al.* 2019), to oscillating driving flows in microfluidic systems (Morris 2001; Vedel, Olesen & Bruus 2010; Ding 2023), etc. The time-dependent velocity field introduces additional complexity compared with the case with a steady flow. Understanding the interplay between diffusion and temporal advection is crucial for predicting and controlling transport processes in various applications. Taylor dispersion theory (Taylor 1953) provides a fundamental analytical tool for characterising the overall transport processes.

The study of the long-time asymptotic dispersion regime for time-dependent flows can date back to the 1960s. Aris (1960) initiated the first analytical investigation of Taylor dispersion in an oscillatory tube flow. He used the classical method of concentration moments proposed by himself (Aris 1956) to derive the expression of Taylor coefficient and revealed the fundamental effect of the flow pulsation. The key to the long-time asymptotic solution is the derivation of the purely periodic part of the first-order moment. The development of the moment method was promoted by Brenner & Edwards (1993), who proposed the generalised Taylor dispersion theory that can be applied to not only time-dependent flows but also to extensions with unsteady components in transport flux. Alternative methods include using the special solution of concentration distribution to directly derive Taylor dispersivity for oscillatory flows, e.g. a linearly longitudinal distribution (although not physically sound for infinitely long channels) (Bowden 1965; Chatwin 1975; Watson 1983; Pedley & Kamm 1988; Mederos *et al.* 2020) and Gaussian distribution for unbounded linear shear flow (Smith 1982*b*; Young, Rhines & Garrett 1982). Nevertheless, crucial experimental verification has been undertaken by many researchers (Joshi *et al.* 1983; Jensen *et al.* 2009; Song & Law 2015; Nissan, Dror & Berkowitz 2017), and more recently by Ding *et al.* (2021) and Elhanati, Dror & Berkowitz (2023).

Another classical method, the multiscale expansion technique, has also been applied to analyse the long-time asymptotic dispersion coefficient of solute transport in oscillatory flows. Fife & Nicholes (1975) first introduced a two-time-scale general asymptotic solution form of concentration distribution for dispersion problems, which can also treat a time-dependent velocity field. Pavliotis (2002) used the typical two-scale homogenisation method (Pavliotis & Stuart 2008) to derive the Taylor dispersion coefficient for periodic flows. Ng (2004, 2006) applied the multiple-time-scale homogenisation method (Mei *et al.* 1996) proposed by Mei (1992) to study the cases of time-periodic channel flows and tube flows with reversible solute adsorption at the walls. The principles behind these multiscale methods are analogous, although with differences in the specific expansion forms and the selection of scales (Camassa, Lin & McLaughlin 2010; Wu & Chen 2014; Ding *et al.* 2021). Recent progress and applications have focused on complex oscillatory transport problems (Barik & Dalal 2019; Chu *et al.* 2019; Ding *et al.* 2021; Karmakar, Barik & Raja Sekhar 2023; Poddar *et al.* 2024).

Recently, the transient dispersion process in time-dependent flows has attracted more interest than the exhaustively explored long-time asymptotic dispersion regime does (Vedel & Bruus 2012). The main focus is the complicated temporal evolution of

https://doi.org/10.1017/jfm.2026.11292 Published online by Cambridge University Press

the Taylor–Aris dispersion coefficient. Thus, the method of concentration moments is probably the remaining viable option for analytical studies. We remark that although the Taylor–Gill generalised dispersion model (Gill & Sankarasubramanian 1971) has also been employed by many studies for various oscillatory flows (Gaver & Grotberg 1990; Hazra, Gupta & Niyogi 1996; Rana & Murthy 2016; Wang & Chen 2017*b*; Singh & Murthy 2023), this method can be considered as a kind of cumulant (alternative to moments) expansion technique (Frankel & Brenner 1991; Jiang & Chen 2018). Indeed, the coefficients in Gill's model can be expressed in moments. Consequently, we will focus on the concentration moment method.

The method of concentration moments is well developed for transport problems with steady flows. Barton (1983) has derived the general expressions for the full transient solution of moments up to the third order (Aquino 2024), using the method of separation of variables (based on the solution by Aris 1956). However, for unsteady flows, these results cannot be applied directly. In fact, the time-dependent velocity makes the solution procedure of moments much more cumbersome. In the ordinary differential equations of the expansion coefficients obtained by separation of variables, the coefficient matrix is time-dependent (i.e. the system is non-autonomous) and thus it can considerably increase the complication of the procedure.

Nevertheless, many researchers have aimed to solve the complete concentration moments in time-periodic flows. Yasuda (1982, 1984) used the method of Green's function to derive the explicit analytical expressions of moments up to the second order for oscillatory currents. Smith (1983) obtained the statistics of concentration moments by a Hermite-series representation of concentration distribution. Dentz & Carrera (2003, 2005) developed the approximate solutions of the drift and dispersivity for temporally fluctuating flows, using the Fourier transform and perturbative analysis framework by Attinger *et al.* (1999). Mukherjee & Mazumder (1988) introduced a so-called time-dependent 'eigenvalue' problem to extend the approach of Barton (1983) to oscillatory flows, using tube and channel flows as examples. The 'eigenvalue' problem is in fact in the same form as the cell problem (i.e. the long-time asymptotic local transport problem) derived in the homogenisation method. In addition, this form of time-dependent eigenvalue problem was proposed by Shapiro & Brenner (1990) based on Brenner's generalised dispersion theory, despite the lack of intuitiveness. They pointed out that the eigenvalues could be complex numbers and the eigenfunctions were time-periodic (Shapiro & Brenner 1987). Only the zeroth-order moment was discussed for its complete time-dependent solution form, while the higher-order moments were sought in their long-time asymptotic form. Actually, if one imposes a new time variable for the oscillatory velocity field, the physical interpretation and the solution structure of the 'eigenvalue' problem will be fundamentally clear. This is the primary aim of our work.

More recently, the method of concentration moments has been extended and applied to the study of transient dispersion in complex oscillatory flows. Vedel & Bruus (2012) extended earlier studies on single-frequency harmonic pulsatile flows (e.g. the work of Mukherjee & Mazumder 1988) to encompass the case of multiple-frequency flows (but with the same base frequency). A trial expansion form has been constructed to seek the full solution of the first-order concentration moment. Later, they studied the transient dispersion with a point-source release (Vedel, Hovad & Bruus 2014). For environmental dispersion in tidal wetland flows, Zeng *et al.* (2012) applied the integral transformation technique to derive the explicit expression for the time-dependent dispersion coefficient, inspiring many subsequent studies (Wu *et al.* 2012; Wang & Chen 2015; Das *et al.* 2024*a*). A later comprehensive study by Ding *et al.* (2021) revisited the transport problem in wall-driven flows (Stokes layer) (Bandyopadhyay & Mazumder 1999; Paul & Mazumder

https://doi.org/10.1017/jfm.2026.11292 Published online by Cambridge University Press

2008). They solved the moment equations up to the third order using series expansions. The analytical results agreed well with their numerical simulations and experimental data.

Apart from the dispersion coefficient, Ding *et al.* (2021) have made the first analytical attempt (to the best of our knowledge) to investigate the temporal evolution of skewness, a fundamental higher-order statistic that reflects the asymmetry of concentration distribution (Chatwin 1970; Aminian *et al.* 2015, 2016). They also analysed the long-time asymptotic behaviour of skewness: the decay rate for a single-frequency flow is $t^{-3/2}$, instead of $t^{-1/2}$ for the steady case (Ding *et al.* 2021, (28)). This observation is in agreement with the asymptotic analysis by Smith (1982*a*, 1983).

Although the general solution expression of skewness has been provided by Ding *et al.* (2021) for arbitrary time-dependent flows, the derivation was based on a specific initial condition, i.e. an instantaneous and uniform source release over the cross-section, such that the zeroth-order concentration moment is 1 and the solution procedure can be greatly simplified. Thus, there remains a fundamental need to tackle general initial conditions, particularly for the case with a point-source release. The corresponding solution can then serve as a Green function (Shapiro & Brenner 1990) for arbitrary release scenarios. Vedel *et al.* (2014) have investigated the effect of point-source position on the dispersion coefficient. However, its effect on the higher-order statistics including skewness has not been analytically studied for oscillatory flows.

Kurtosis, another useful higher-order statistic to characterise the deviation of concentration distribution from Gaussian distribution, was not addressed by Ding *et al.* (2021), probably due to the complication introduced by the oscillatory nature of the velocity field. The long-time asymptotic behaviour of kurtosis has been discussed by Smith (1983), concluding that the decay rate for oscillatory flows is t^{-1}, the same as that for steady flows (Chatwin 1972). Although for the steady flows, many researchers have analytically investigated the transient evolution of kurtosis (Andersson & Berglin 1981; Aminian *et al.* 2015; Wang & Chen 2017*a*; Guo *et al.* 2022), little analytical work has been done for time-periodic flows. Previous studies had to resort to numerical methods to calculate the high-order moments for kurtosis (Allen 1982; Mazumder & Das 1992; Debnath *et al.* 2019). For example, recent studies by Dhar *et al.* (2022) and Das *et al.* (2024*b*) have applied the finite-difference method to numerically solve the governing equations of moments up to the fourth order.

Recently, Singh & Murthy (2023) and Pal, Singh & Murthy (2025) have derived an integral-form expression of kurtosis. Their comprehensive and systematic studies have applied the method of concentration moments to investigate the transport problem in pulsating non-Newtonian fluid flows. They found that the kurtosis of the case with oscillatory flows, similar to skewness, can also be much smaller than that of steady flows, implicating that the concentration distribution may become Gaussian faster for the oscillatory flows than for steady flows (Mazumder & Das 1992).

Although the integral-form expression of kurtosis has been obtained, it should be noted that the solution expression is inexplicit: it contains a lot of unsolved nested symbolic integrals with respect to time. This can be seen in (D5)–(D8) in the work of Singh & Murthy (2023), where four forms of integrals were defined hierarchically. Analytically solving these nested integrals up to the last-order is a challenging task. In fact, they numerically calculated the integration of these integrals, using Simpson's 1/3 rule. This numerical solution procedure was previously used by Rana & Murthy (2016). As a comparison, the solution expression of the third-order concentration moment by Ding *et al.* (2021) is fully explicit with respect to the time variable (i.e. no unsolved symbolic integrals). Thus, there remains a need to explicitly solve the fourth-order moment for kurtosis.

https://doi.org/10.1017/jfm.2026.11292 Published online by Cambridge University Press

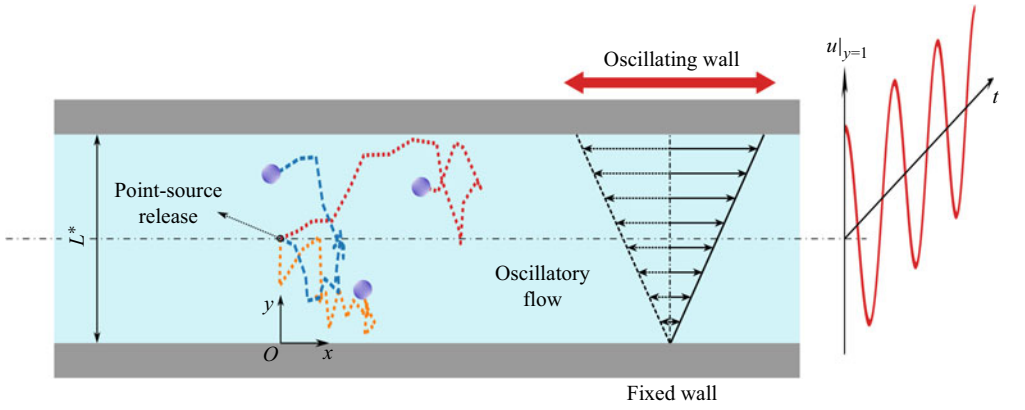


Figure 1. Sketch of solute transport problem in an oscillatory flow created by the oscillating channel wall. Several simulated particle trajectories are shown. The time variable in the oscillatory velocity field can be virtually viewed as an additional 'transverse' spatial variable.

This study aims to address the issue of the complication induced by the time-periodic velocity field during the analytical solution procedure of concentration moments, especially when solving for higher-order statistics such as skewness and kurtosis. We introduce a new auxiliary time variable for the oscillatory velocity field and extend the original transport problem to a two-time-variable problem (which is analogous to the multi-time scale method). To some extent, the new time dimension can be virtually viewed as an additional 'transverse' periodic space. This treatment can not only offer an intuitive physical perspective on the effects of velocity field oscillation on dispersion, but also clarify the structure of the governing equations of moments. More importantly, under this new two-time-variable transport problem, there is no need to re-solve the moment equation. The general solution expressions obtained by Barton (1983) for steady flows can be directly applied to the case of oscillatory flows, because the flow velocity becomes 'steady' after 'splitting' the time variable. The remaining procedure simply involves: (i) identifying the new eigenvalue problem and (ii) substituting the eigenvalues and eigenfunctions into Barton's expressions. Therefore, the complications encountered in previous methods can be avoided. It is feasible to analytically investigate the temporal evolution of higher-order statistics for time-periodic flows, analogous to the steady-flow case.

2. Formulation of transport problem and concentration moments

2.1. *Governing equation*

To illustrate the analytical solution procedure, we consider mass transport in a parallel channel with a time-dependent velocity field. For simplicity, we focus on the two-dimensional transport problem. A typical case is shown in figure 1.

The dimensionless form of the whole transport problem can be adopted as follows:

$$\frac{\partial C}{\partial t} + u(y,t)\frac{\partial C}{\partial x} = \frac{1}{Pe^2}\frac{\partial^2 C}{\partial x^2} + \frac{\partial^2 C}{\partial y^2}, \tag{2.1a}$$

$$\left.\frac{\partial C}{\partial y}\right|_{y=0} = \left.\frac{\partial C}{\partial y}\right|_{y=1} = 0, \tag{2.1b}$$

$$C|_{t=0} = C_{ini}(y)\delta(x). \tag{2.1c}$$

https://doi.org/10.1017/jfm.2026.11292 Published online by Cambridge University Press

The range of the dimensionless variables is $-\infty < x < +\infty$ (the channel length is infinite), $0 < y < 1$ (the dimensionless channel width is 1) and $t > 0$ (the time). Note that the following dimensionless parameters and variables have been chosen (the superscript asterisk denotes dimensional variables and parameters):

$$x = \frac{1}{Pe}\frac{x^*}{L^*}, \quad y = \frac{y^*}{L^*}, \quad t = \frac{t^*}{L^{*2}/D^*},$$
$$u = \frac{u^*}{U_c^*}, \quad C = Pe\frac{C^*}{C_c^*}, \quad Pe = \frac{U_c^* L^*}{D^*}, \quad \omega = \frac{\omega^*}{D^*/L^{*2}}, \tag{2.2}$$

where L^* is the channel width, D^* is the solute diffusion coefficient, U_c^* is a characteristic velocity and Pe is the corresponding Péclet number. Here, C_c^* is a characteristic concentration constant such that the dimensionless concentration distribution satisfies

$$\int_{-\infty}^{\infty}\int_0^1 C(x, y, t)\,\mathrm{d}y\,\mathrm{d}x = 1. \tag{2.3}$$

Namely, C is a well-defined probability density function.

For the advection term in (2.1*a*), the dimensionless time-dependent flow velocity $u(y, t)$ is assumed to be oscillatory and the dimensionless angular frequency is ω. Namely, the dimensionless period of the flow velocity $T = 2\pi/\omega$ and

$$u(y, t + T) = u\left(y, t + \frac{2\pi}{\omega}\right) = u(y, t). \tag{2.4}$$

Equation (2.1*b*) is the non-penetration boundary condition. Equation (2.1*c*) is the initial condition. The solute is assumed to be instantaneously released in a cross-section of the channel. Here, δ denotes the Dirac delta function and $C_{ini}(y)$ is initial transverse distribution.

2.2. *Concentration moments*

The goal of this study is to derive the complete time-dependent solution of concentration moments for the above-mentioned transport problem with unsteady flow velocity. First, we follow the work by Aris (1956) to define the nth-order concentration moment for $C(x, y, t)$ as

$$C_n(y, t) \triangleq \int_{-\infty}^{\infty} x^n C(x, y, t)\,\mathrm{d}x \tag{2.5}$$

for $n = 0, 1, 2, \ldots$. The moments of the cross-sectional mean concentration distribution are more practical in applications. Here, we use the bar to denote variables related to the cross-sectional mean concentration distribution and

$$\bar{C}(x, t) \triangleq \int_0^1 C(x, y, t)\,\mathrm{d}y. \tag{2.6}$$

Similarly, the nth order moment of $\bar{C}$ is defined as

$$\bar{C}_n(t) \triangleq \int_{-\infty}^{\infty} x^n \bar{C}(x, t)\,\mathrm{d}x \tag{2.7}$$

for $n = 0, 1, 2, \ldots$.

The first four order moments are related to the most fundamental overall characteristics of the solute transport problem. Here, $\bar{C}_0$ represents the total amount of solute mass and

https://doi.org/10.1017/jfm.2026.11292 Published online by Cambridge University Press

$\bar{C}_0 = 1$ for the current transport problem. The averaged moving speed of the solute cloud, i.e. the drift, is

$$u_d \triangleq \frac{\mathrm{d}\overline{\mu_x}}{\mathrm{d}t} = \frac{\mathrm{d}}{\mathrm{d}t}\left(\frac{\bar{C}_1}{\bar{C}_0}\right) = \frac{\mathrm{d}\bar{C}_1}{\mathrm{d}t}, \tag{2.8}$$

where $\overline{\mu_x}$ is the mean position of the solute cloud (expected value).

The effective diffusion (apparent dispersivity) is related to the second-order moment $\bar{C}_2$ as

$$D_e \triangleq \frac{1}{2}\frac{\mathrm{d}\bar{\sigma}^2}{\mathrm{d}t} = \frac{1}{2}\frac{\mathrm{d}}{\mathrm{d}t}\left(\frac{\bar{C}_2}{\bar{C}_0} - \frac{\bar{C}_1^2}{\bar{C}_0^2}\right) = \frac{1}{2}\frac{\mathrm{d}}{\mathrm{d}t}(\bar{C}_2 - \bar{C}_1^2), \tag{2.9}$$

where $\bar{\sigma}^2$ is the variance of the mean concentration distribution.

The higher-order statistics including skewness and kurtosis are also of interest because they can basically reflect the deviation from a Gaussian distribution. Skewness is a measure of the asymmetry of the longitudinal concentration distribution, whose definition is related to the third-order moment $\bar{C}_3$ as

$$Sk \triangleq \frac{\bar{\kappa}_3}{\bar{\sigma}^3} = \frac{\bar{C}_3 - 3\bar{C}_1\bar{C}_2 + 2\bar{C}_1^3}{\bar{\sigma}^3}, \tag{2.10}$$

where $\bar{\kappa}_3$ is the third-order cumulant.

Kurtosis (excess kurtosis) is a measure of the outliers of a distribution (the tail weight) compared with a Gaussian distribution. One can use the fourth-order cumulant $\bar{\kappa}_4$ to define the excess kurtosis as

$$Ku \triangleq \frac{\bar{\kappa}_4}{\bar{\sigma}^4} = \frac{\bar{C}_4 - 4\bar{C}_1\bar{C}_3 - 3\bar{C}_2^2 + 12\bar{C}_1^2\bar{C}_2 - 6\bar{C}_1^4}{\bar{\sigma}^4}. \tag{2.11}$$

Therefore, we need the fourth-order moment $\bar{C}_4$.

Typically, the next step of the method of concentration moments is to derive the governing equations of moments and then solve them order by order (see the paper by Ding *et al.* 2021 for details). The governing equation of moments C_n for the current transport problem is given in Appendix A. However, due to the time-dependent velocity field, the tedious treatment of the time integral with the oscillation terms is a key issue (cf. Singh & Murthy 2023, with (D5)–(D8) numerically integrated). The corresponding solution procedure is much more complicated than that of the steady-flow case, making it difficult to obtain the complete explicit expressions for higher-order moments. Therefore, we will not solve the original moment equations. Instead, we introduce an associated two-time-variable transport problem to get rid of the time-dependent velocity field.

3. Auxiliary-time extension method

Here, a new method is proposed to solve the concentration moments. Analogous to the multi-time scale method, an auxiliary time variable associated with the oscillation frequency of the flow is devised to characterise the intrinsic oscillation in the dispersion. By extending the original transport problem to a two-time-variable problem, the time-dependent velocity becomes 'steady' with the basic time variable while time-dependant only in the auxiliary time dimension. This key treatment enables us to directly apply the general solution expressions obtained by Barton (1983) for steady flows to the case of oscillatory flows. Generally speaking, it is not necessary to independently re-solve the oscillatory problem.

https://doi.org/10.1017/jfm.2026.11292 Published online by Cambridge University Press

3.1. *Two-time-variable system*

First, we impose a two-time-variable system with

$$t_0 = t, \quad t_1 = \omega t. \tag{3.1}$$

While t_0 represents the original basic time, the new auxiliary time t_1, referred to as oscillation time, is introduced directly associated with the frequency ω of the oscillating flow to characterise the inherent oscillation in the dispersion. Thus, the oscillatory velocity is only relevant to t_1. For convenience, we define a new velocity function of t_1 as

$$u_1(y, t_1) \triangleq u\left(y, \frac{t_1}{\omega}\right) = u(y, t), \tag{3.2}$$

such that we can simply replace $u(y, t)$ with $u_1(y, t_1)$ in the original transport equation (2.1*a*). Note that u_1 is a periodic function of t_1 with a period of 2π.

Next, the concentration distribution $C(x, y, t)$ needs to be extended to some virtual 'concentration' function in the two-time-variable system, denoted as $P(x, y, t_0, t_1)$. The relationship between C and P is

$$C(x, y, t) = P(x, y, t_0 = t, t_1 = \omega t). \tag{3.3}$$

Note that there may exist many possible extensions from C to P in the higher-dimensional system. One of the most straightforward choices is to set P periodic with respect to t_1 because t_1 is the oscillation time and, thus, it requires

$$P(x, y, t_0, t_1) = P(x, y, t_0, t_1 + 2\pi). \tag{3.4}$$

For the time derivative, using the chain rule, we have

$$\frac{\partial C}{\partial t} = \frac{\partial P}{\partial t_0} + \frac{\partial P}{\partial t_1}\frac{\partial t_1}{\partial t} = \frac{\partial P}{\partial t_0} + \omega\frac{\partial P}{\partial t_1}. \tag{3.5}$$

Readers may find that the above-mentioned two-time-variable procedure is similar to the two-time-scale homogenisation method used in 'previous studies (e.g. Ding *et al.* 2021). In fact, if one replaces ω with a so-called small perturbation parameter ϵ, then the formulations are the same. However, we would not dive into the perturbation analysis with the multi-scale expansion of concentration. More importantly, the angular frequency of the velocity in this study is not required to be confined as in the two-scale method. Neither a small parameter nor scale analysis is needed. Thus, we use the term 'two-time variable' instead of 'two-time scale'. What we are looking for is the complete solution of concentration moments, not the long-time asymptotic concentration distribution (which is the focus of the homogenisation method). Our work finds that the two-time variable formulation could provide a new perspective for the analytical solution of concentration moments. We have compared the analytical result by the two-time variable method with numerical results for different magnitude values of parameters, see figures 3 and 9.

3.2. *Governing equation for the two-time-variable system*

Equation (3.3) offers the relationship between C and P. Substituting P into the transport equation (2.1*a*) and using the time derivatives in (3.5), we can obtain the governing equation for P as

$$\frac{\partial P}{\partial t_0} + \omega\frac{\partial P}{\partial t_1} + u_1(y, t_1)\frac{\partial P}{\partial x} = \frac{1}{Pe^2}\frac{\partial^2 P}{\partial x^2} + \frac{\partial^2 P}{\partial y^2}. \tag{3.6}$$

Apparently, the second term on the left side reflects the auxiliary flux change due to periotic oscillation in the oscillation time dimension t_1, actually a translation effect in

https://doi.org/10.1017/jfm.2026.11292 Published online by Cambridge University Press

the oscillation space, with the oscillation frequency standing for the translation speed in the oscillation time dimension. When $\omega = 0$, i.e. for the steady case, the form of (3.6) for P is the same as the original (2.1*a*) for C.

Because P is periodic with respect to t_1 as in (3.4), we can confine the whole problem within one periodic interval $[0, 2\pi]$ of t_1. Namely, t_1 is with the modulus 2π,

$$t_1 = (\omega t) \mod 2\pi, \tag{3.7}$$

then we can impose the following periodic conditions with respect to t_1 for P:

$$P|_{t_1=0} = P|_{t_1=2\pi}. \tag{3.8}$$

It is further required that P represents the 'probability density function' in the two-time-variable system (within one period of t_1), namely,

$$\int_{-\infty}^{\infty}\int_{0}^{1}\int_{0}^{2\pi} P(x, y, t_0, t_1)\,\mathrm{d}t_1\,\mathrm{d}y\,\mathrm{d}x = 1. \tag{3.9}$$

We can define the probability moment of P in § 3.3.

The boundary condition of P at the channel walls is the same as that of C in (2.1*b*),

$$\left.\frac{\partial P}{\partial y}\right|_{y=0} = \left.\frac{\partial P}{\partial y}\right|_{y=1} = 0. \tag{3.10}$$

To complete the transport problem of P in the two-time-variable system, an 'initial' condition at $t_0 = 0$ is needed. According to the initial condition (2.1*c*) of C, the simplest choice for P is

$$P|_{t_0=0} = C_{ini}(y)\delta(x). \tag{3.11}$$

Namely, the initial condition is independent of t_1. In fact, we just set the initial condition for P to satisfy

$$C(x, y, t = 0) = P(x, y, t_0 = 0, t_1 = 0), \tag{3.12}$$

and $P|_{t_0=0}$ is periodic with respect to t_1.

We have obtained the whole initial-boundary value problem (3.6), (3.8), (3.10), (3.11) of P in the two-time-variable system. If a solution of P is given, then through (3.3), the solution of C can be immediately obtained because it satisfies all the equations in the transport problem (2.1) for C. However, obtaining the exact solution of P is challenging, as is the case for C. Therefore, we consider the concentration moments instead, as in § 2.2.

3.3. *Probability moments*

Similar to the definition of concentration moment in (2.5), one can also define the moments of $P(x, y, t_0, t_1)$ and then obtain the corresponding moment equations. The nth-order probability moment is

$$P_n(y, t_0, t_1) \triangleq \int_{-\infty}^{\infty} x^n P(x, y, t_0, t_1)\,\mathrm{d}x \tag{3.13}$$

for $n = 0, 1, 2, \ldots$. According to the relationship (3.3) between P and C, we have the relationship between P_n and C_n,

$$C_n(y, t) = P_n(y, t_0 = t, t_1 = \omega t). \tag{3.14}$$

Namely, once we solve P_n, the solution for C_n can be immediately obtained.

https://doi.org/10.1017/jfm.2026.11292 Published online by Cambridge University Press

According to (3.6), (3.8), (3.10), (3.11), the whole initial-boundary value problem for P_n is

$$\frac{\partial P_n}{\partial t_0} + \omega \frac{\partial P_n}{\partial t_1} - \frac{\partial^2 P_n}{\partial y^2} = n\, u_1(y, t_1) P_{n-1} + \frac{n(n-1)}{Pe^2} P_{n-2}, \tag{3.15a}$$

$$P_n|_{t_1=0} = P_n|_{t_1=2\pi}, \tag{3.15b}$$

$$\left.\frac{\partial P_n}{\partial y}\right|_{y=0} = \left.\frac{\partial P_n}{\partial y}\right|_{y=1} = 0, \tag{3.15c}$$

$$P_n|_{t_0=0} = \begin{cases} C_{ini}(y), & n = 0, \\ 0, & n = 1, 2, \ldots, \end{cases} \tag{3.15d}$$

with auxiliary terms $P_{-1} = P_{-2} = 0$.

3.4. *Eigenvalue problem*

In the two-time-variable system, the governing equation (3.15*a*) of moments for the oscillatory flow is similar to the case of a steady flow because t_1 can be viewed as a spatial variable and the velocity is independent of t_0. Therefore, now we are able to directly apply the generic solution expressions of moments given by Barton (1983, 1984) for the case of steady flows. The key is to solve the corresponding eigenvalue problem to determine the eigenvalues and eigenfunctions in Barton's expressions.

According to (3.15), the complete eigenvalue problem for probability moment P_n is

$$-\omega \frac{\partial f}{\partial t_1} + \frac{\partial^2 f}{\partial y^2} = -\lambda f, \tag{3.16a}$$

$$f|_{t_1=0} = f|_{t_1=2\pi}, \tag{3.16b}$$

$$\left.\frac{\partial f}{\partial y}\right|_{y=0} = \left.\frac{\partial f}{\partial y}\right|_{y=1} = 0, \tag{3.16c}$$

where λ is an eigenvalue and $f = f(y, t_1)$ is the corresponding eigenfunction.

As mentioned in the introduction, we remark that Mukherjee & Mazumder (1988, (3.1)) have introduced a similar 'eigenvalue' problem (time-dependent) to extend Barton's method to oscillatory flows. Furthermore, Shapiro & Brenner (1990, (16) and (17)) proposed the same form of the time-dependent problem. They pointed out that the eigenvalue problem is non-self-adjoint and gave the full solution form of the zeroth-order moment.

The fundamental difference we make here is the introduction of the oscillation time variable t_1 to make the oscillatory flow 'steady' with respect to time variable t_0. The eigenvalue problem (3.16) is thus independent of time t_0, intrinsically different from the time-dependent one discussed by Mukherjee & Mazumder (1988) and Shapiro & Brenner (1990). Thus, the introduction of t_1 not only enables one to use Barton's result directly, but also can clarify the solution structure of moments (cf. § 6).

The eigenvalue problem (3.16) can be solved using the complex form of Fourier series. The solution of eigenfunction can be written as (see also Appendix B)

$$f_{m,k}(y, t_1) = A_m \cos(m\pi y) \frac{1}{\sqrt{2\pi}} \mathrm{e}^{\mathrm{i}kt_1}, \tag{3.17}$$

where indices $k = 0, \pm 1, \pm 2, \ldots$ for non-zero ω, and $m = 0, 1, 2, \ldots$. When $\omega = 0$ for the steady case, we keep $k = 0$ and then the whole solution framework reduces to Barton's formulation. The imaginary unit is i and $\mathrm{i}^2 = -1$. The factor $1/\sqrt{2\pi}$ for the Fourier series

https://doi.org/10.1017/jfm.2026.11292 Published online by Cambridge University Press

of t_1 and the undermined coefficient A_m for the function of y is used for the normalisation condition (3.20).

The corresponding eigenvalue is

$$\lambda_{m,k} = (m\pi)^2 + \mathrm{i}\omega k. \tag{3.18}$$

Namely, the 'eigenvalue' can be a complex number instead of a real number, because the eigenvalue problem can be non-self-adjoint.

The inner product for the eigenvalue problem is defined as

$$\langle f_1,\, f_2\rangle \triangleq \int_0^{2\pi}\int_0^1 f_1^\star(y,t_1)\, f_2(y,t_1)\,\mathrm{d}y\,\mathrm{d}t_1, \tag{3.19}$$

where f_1 and f_2 are arbitrary functions. The superscript $\star$ denotes the complex conjugate. Note that due to the complex form of Fourier series, the orthonormal relationship (orthogonal and normalised) between eigenfunctions can be obtained:

$$\langle f_{m_1,k_1},\, f_{m_2,k_2}\rangle = \delta_{m_1m_2}\delta_{k_1k_2}, \tag{3.20}$$

because

$$\int_0^{2\pi}\left(\frac{1}{\sqrt{2\pi}}\mathrm{e}^{\mathrm{i}k_1t_1}\right)^\star \frac{1}{\sqrt{2\pi}}\mathrm{e}^{\mathrm{i}k_2t_1}\,\mathrm{d}t_1 = \frac{1}{2\pi}\int_0^{2\pi}\mathrm{e}^{\mathrm{i}(-k_1+k_2)t_1}\,\mathrm{d}t_1 = \delta_{0(-k_1+k_2)} = \delta_{k_1k_2}. \tag{3.21}$$

Here, δ_{ij} is the Kronecker delta,

$$\delta_{ij} = \begin{cases} 1, & i = j,\\ 0, & i \neq j. \end{cases} \tag{3.22}$$

3.5. *Solutions of moments*

The final step of solving P_n is to substitute the eigenvalues (3.18) and eigenfunctions (3.17) into the generic solution expressions of Barton (1983, 1984). Some recent applications (Wang & Chen 2017*a*; Yang *et al.* 2021; Jiang *et al.* 2022) have also given detailed expressions. Because the expressions are similar (only the notation is different), here, we just discuss P_0 and P_1 as illustrative examples, while the solutions of the higher-order moments are given in Appendix C. We mainly follow § 4.4 of Jiang *et al.* (2022) and reformulate the solution expressions using the current notation.

First, we can reindex the eigenvalues and eigenfunctions for convenience. Note that due to the introduction of t_1, there are two indices m and k for the eigenfunctions ($f_{m,k}(y,t_1)$, with two dimensions). Hereafter, we use index i for the list of eigenfunctions $\{f_i(y,t_1)\}_{i=0}^{\infty}$ and the list of eigenvalues $\{\lambda_i\}_{i=0}^{\infty}$, sorted in the ascending order of the absolute value of $\lambda_{m,k}$. The list will then be truncated at a finite number when evaluating the series summation in the following solution expressions. Notice that the index i should not be confused with the imaginary unit i.

For the zeroth-order moment, based on (3.1) of Barton (1983),

$$P_0(y,t_0,t_1) = \sum_{i=0}^{\infty} a_i\mathrm{e}^{-\lambda_i t_0} f_i(y,t_1), \tag{3.23}$$

where a_i is the coefficient related to the initial condition,

$$a_i \triangleq \langle f_i,\, P_0|_{t_0=0}\rangle = \int_0^{2\pi}\int_0^1 f_i^\star(y,t_1)C_{ini}(y)\,\mathrm{d}y\,\mathrm{d}t_1, \quad i = 0,1,\ldots. \tag{3.24}$$

https://doi.org/10.1017/jfm.2026.11292 Published online by Cambridge University Press

Note that the initial condition (3.15*d*) is independent of t_1 and thus the coefficient a_i for the oscillatory term with t_1 is zero, namely, there is no oscillation in (3.23). Although we introduce a more complicated function base ($f_i(y, t_1)$), P_0 is independent of t_1. In addition, according to (3.14), the oscillatory term in $\mathrm{e}^{-\lambda_i t_0}$ is cancelled out with the term of t_1 in $f_i(y, t_1)$, namely, $\mathrm{e}^{-\mathrm{i}\omega k t_0}\mathrm{e}^{\mathrm{i}k t_1} = 1$. We obtain the same conclusion: no oscillation for P_0. This is not surprising because the zeroth-order moment is the total amount of mass in each parallel streamline (cf. the concept of streamwise dispersion (Guan & Chen 2024)), which is not affected by the oscillatory flow.

For the first-order moment P_1, based on (2.9) by Barton (1984) (here, we recollect the terms with respect to f_i and $t_0 f_i$),

$$P_1(y, t_0, t_1) = t_0 \sum_{i=0}^{\infty} a_i B_{i,i} \mathrm{e}^{-\lambda_i t_0} f_i(y, t_1) + \sum_{\substack{i,j=0 \\ j\neq i}}^{\infty} \frac{a_j B_{i,j}(\mathrm{e}^{-\lambda_j t_0} - \mathrm{e}^{-\lambda_i t_0})}{\lambda_i - \lambda_j} f_i(y, t_1), \tag{3.25}$$

where $B_{i,j}$ is the expansion coefficient related to the inner product with the velocity profile,

$$B_{i,j} \triangleq \langle f_i, u_1 f_j \rangle = \int_0^{2\pi} \int_0^1 f_i^{\star}(y, t_1) u_1(y, t_1) f_j(y, t_1)\, \mathrm{d}y\, \mathrm{d}t_1 \tag{3.26}$$

for $i, j = 0, 1, \ldots$. Similar to P_0, note that the first term in (3.25) is independent of t_1. The second term may be oscillatory because it contains $a_j B_{i,j} \mathrm{e}^{-\lambda_j t_0} f_i(y, t_1)$ (when $i \neq j$).

Note that in practice, the oscillatory velocity profile can be generally expressed in the form of the Fourier series of t_1 (or t in the original transport problem). Therefore, the following formula for the integration of the product of three eigenfunctions with respect to t_1 can be helpful,

$$\int_0^{2\pi} \frac{1}{\sqrt{2\pi}} \mathrm{e}^{\mathrm{i}k_1 t_1} \frac{1}{\sqrt{2\pi}} \mathrm{e}^{\mathrm{i}k_2 t_1} \frac{1}{\sqrt{2\pi}} \mathrm{e}^{\mathrm{i}k_3 t_1}\, \mathrm{d}t_1 = \frac{1}{\sqrt{2\pi}} \delta_{0(k_1+k_2+k_3)}. \tag{3.27}$$

Namely, when $k_1 + k_2 + k_3 = 0$, the integration result is $1/\sqrt{2\pi}$.

The solutions for the second- and higher-order moments P_n are given in Appendix C. Once we solve P_n, the solution for C_n can be immediately obtained through (3.14). Then, the dispersion characteristics can be calculated according to their definitions in § 2.2.

4. Verification with numerical simulation: oscillatory Couette flow

As a first step of verification and illustration of the new method, the oscillatory Couette flow (Stokes–Couette flow), one of the simplest oscillatory flows, is considered. To verify the analytical solution of concentration moments, the numerical results by the Brownian dynamics simulation method are used for comparison.

4.1. *Velocity profile of oscillatory Couette flow*

A sketch of the transport problem is shown in figure 1. See also the recent experiment by Ding *et al.* (2021). The bottom wall ($y^* = 0$) is at rest, while the upper wall ($y^* = L^*$) is executing an oscillatory motion with velocity $U_A^* \cos(\omega^* t^*)$, where U_A^* is the amplitude of the velocity oscillation and ω^* is the angular frequency.

https://doi.org/10.1017/jfm.2026.11292 Published online by Cambridge University Press

Based on the dimensionless parameters and variables in (2.2), we introduce two additional dimensionless parameters:

$$Sc = \frac{\nu^*}{D^*}, \quad Wo = L^* \sqrt{\frac{\omega^*}{\nu^*}}. \tag{4.1}$$

Notice that $\omega = ScWo^2$, where Sc is the Schmidt number and Wo is the Womersley number. Here, ν^* is the kinematic viscosity of the fluid. For the choice of the characteristic velocity in (2.2), we use the velocity oscillation scale, namely $U_c^* = U_A^*$.

The dimensionless Navier–Stokes equation and the boundary conditions for this case are

$$\frac{1}{Sc}\frac{\partial u}{\partial t} = \frac{\partial^2 u}{\partial y^2}, \quad u|_{y=1} = \cos(\omega t), \quad u|_{y=0} = 0. \tag{4.2}$$

The oscillatory velocity profile has a solution (Drazin & Riley 2006; Ding *et al.* 2021):

$$u(y, t) = \mathrm{Re}\left[\mathrm{e}^{\mathrm{i}\omega t} \frac{\sinh\left(\mathrm{e}^{(\pi/4)\mathrm{i}} Woy\right)}{\sinh\left(\mathrm{e}^{(\pi/4)\mathrm{i}} Wo\right)} \right]. \tag{4.3}$$

Notice that $\mathrm{e}^{(\pi/4)\mathrm{i}} = \sqrt{\mathrm{i}} = (\sqrt{2}/2)(1+\mathrm{i})$. Here, Re means taking the real part of the complex number.

For the two-time-variable system (3.6), we need to rewrite the velocity profile (4.3) in the form of the Fourier series of t_1 (see also the definition of u_1 in (3.2)) to calculate the expansion coefficient $B_{i,j}$ in (3.26):

$$u_1(y, t_1) = \sum_{k=\pm 1} \frac{\sqrt{2\pi}}{2} \left[\frac{1}{\sqrt{2\pi}} \mathrm{e}^{\mathrm{i}kt_1} \frac{\sinh\left(\mathrm{e}^{(\pi/4)\mathrm{i}}\sqrt{k}Woy\right)}{\sinh\left(\mathrm{e}^{(\pi/4)\mathrm{i}}\sqrt{k}Wo\right)} \right], \tag{4.4}$$

see also (5) of Ding *et al.* (2021). Note that only one frequency is considered here. For the multiple-frequency case with more Fourier components (see also the paper by Vedel & Bruus 2012), the solution procedure is similar but with more expansion coefficients for the 'time' variable t_1.

Based on the experimental study by Ding *et al.* (2021), we consider the transport problem of illuminated fluorescein dye in water. We perform the numerical simulation and analytical investigation based on the parameters listed in table 1. More cases of different parameter set-ups can be found in figure 9. In this case, the temporal evolution of the velocity profile is shown in figure 2. Due to the small Womersley number, the velocity profile is almost linear along the channel, namely, the boundary layer effect is weak.

4.2. *Comparison with numerical simulation*

To verify our analytical solution of the concentration moments, the Brownian dynamics simulation method (also known as the Monte Carlo method or random walk simulation) is adopted to obtain the numerical solutions. This simulation approach is widely applicable in various fields (Elhanati *et al.* 2023; Wu *et al.* 2026), as discussed in the comprehensive review by Berkowitz *et al.* (2006). The numerical algorithm can be found in the recent paper by Ding *et al.* (2021, § 3) (see also Wang *et al.* 2021, Appendix A; Jiang & Chen 2021, Appendix B).

https://doi.org/10.1017/jfm.2026.11292 Published online by Cambridge University Press

Parameter	Description	Reference value	Unit
L^*	Channel width	1.6×10^{-3}	m
D^*	Diffusion coefficient	8.81×10^{-10}	$\mathrm{m^2\ s^{-1}}$
ω^*	Angular frequency	$2\pi/1500$	$\mathrm{rad\ s^{-1}}$
ν^*	Kinetic viscosity	1.13×10^{-6}	$\mathrm{m^2\ s}$
U_A^*	Amplitude of velocity oscillation	4.19×10^{-5}	$\mathrm{m\ s^{-1}}$
ω	Dimensionless angular frequency	12.17	
Pe	Péclet number	76.07	
Wo	Womersley number	9.74×10^{-2}	
Sc	Schmidt number	1282.63	

Table 1. Dimensional and dimensionless parameters in (2.2) and (4.1) for the transport of illuminated fluorescein dye in an oscillatory Couette flow of water. The parameters are partially taken from the experimental study by Ding *et al.* (2021).

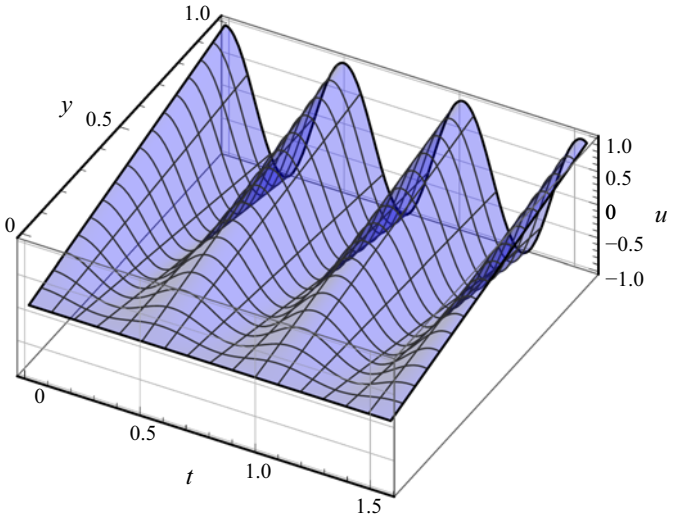


Figure 2. Dimensionless velocity profile $u(y, t)$ of the oscillatory Couette flow with the parameters listed in table 1.

First, we need to find the corresponding stochastic differential equations (SDEs) for the original transport problem (2.1):

$$\mathrm{d}X_t = u(Y_t, t)\,\mathrm{d}t + \frac{\sqrt{2}}{Pe}\,\mathrm{d}W_1, \tag{4.5a}$$

$$\mathrm{d}Y_t = \sqrt{2}\,\mathrm{d}W_2, \tag{4.5b}$$

where X_t and Y_t are the random horizontal and transverse coordinates of the position of a particle, respectively. Here, W_1 and W_2 are independent standard Brownian motions.

In our simulation, the Euler–Maruyama method is adopted to numerically solve the SDEs. The details are given in Appendix D. As shown in figure 8, after checking the independence of the time step (Δt) and the number of particles (N), we take $\Delta t = 10^{-3}$ and $N = 10^5$. For the point-source release considered in figure 3, all particles are initially

https://doi.org/10.1017/jfm.2026.11292 Published online by Cambridge University Press

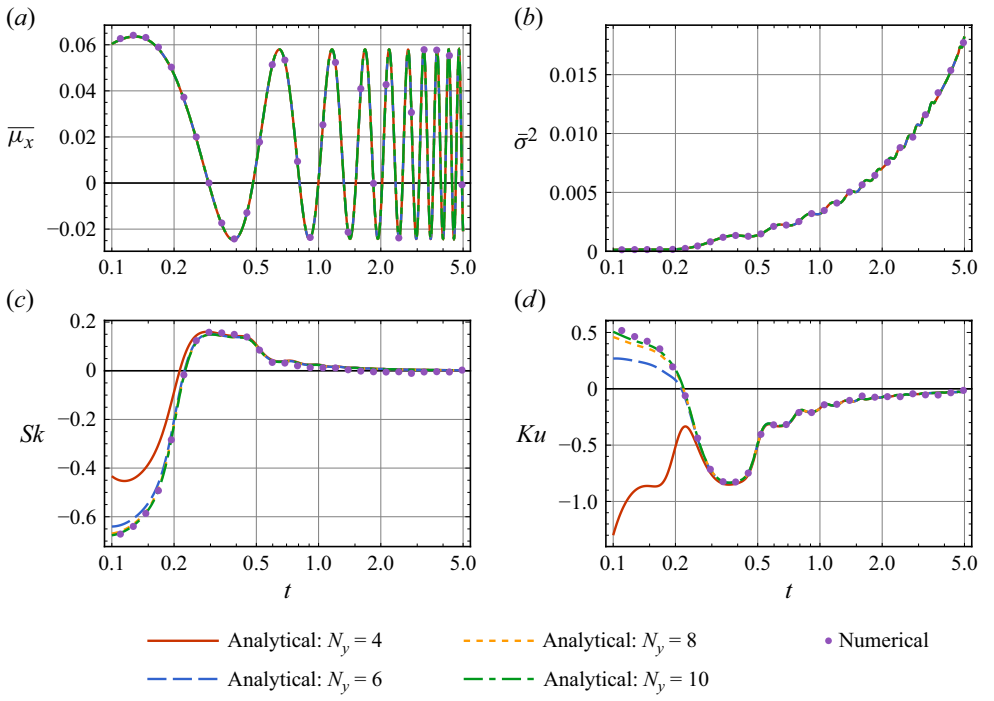


Figure 3. Comparison between the analytical solution of concentration moments and the numerical result by Brownian dynamics simulation: (*a*) the first-order moment of mean concentration distribution; (*b*) the variance of $\bar{C}$; (*c*) the skewness of $\bar{C}$; and (*d*) the kurtosis of $\bar{C}$. N_y denotes the number of eigenfunctions of y used in the truncated summation of the analytical solution. The initial condition is a point-source release at $y_0 = 1$. Other parameters are listed in table 1.

released at $x_0 = 0$ and $y_0 = 1$, which corresponds to

$$C_{ini} = \delta(y - 1) \tag{4.6}$$

in (2.1*c*). The trajectories of particles are recorded. The positions of particles are used to statistically calculate concentration moments.

For the analytical solution, the infinite summations in the solution expressions (such as (3.23)) need to be truncated for calculation or numerical evaluation (Barton 1983). Only the first few eigenvalues (3.18), with indices k and m, and eigenfunctions (3.17) are used for the summations. First, for the Fourier series of t_1 for the oscillation in (3.17), we take $|k| \leqslant 4$ because we only consider concentration moments up to the fourth order for the discussion of kurtosis and the velocity profile is of one frequency. Higher-order moments will require more Fourier components of t_1.

Second, for the trigonometric functions of y in (3.17), the first N_y eigenfunctions of y (i.e. $m \leqslant N_y - 1$, because m starts from 0) are used. We check the accuracy of the truncated summations by comparing the results of $N_y = 4, 6, 8, 10$. Take $N_y = 8$ as an example. The total number of eigenfunctions $f_{m,k}$ is $8 \times (2 \times 4 + 1) = 72$. Then, we recollect all the eigenfunctions and eigenvalues into single-indexed lists $\{f_i(y, t_1)\}_{i=0}^{71}$ and $\{\lambda_i\}_{i=0}^{71}$, and substitute them into the solution expressions of concentration moments.

As shown in figure 3, the analytical solutions of the transport characteristics of the mean concentration distribution $\bar{C}$ agree well with the numerical results, showing the correctness of the proposed auxiliary-time extension procedure. More comparisons under different parameter set-ups can be found in figure 9.

https://doi.org/10.1017/jfm.2026.11292 Published online by Cambridge University Press

The truncation error may be large when t is small, because a point-source-release initial condition (4.6) is considered. As shown in figure 3(c, d) for skewness and kurtosis, the curves of the results with $N_y = 4$ and $N_y = 6$ deviate from the numerical results in the initial stage. Namely, more eigenfunctions may be required for the higher-order moments. Generally speaking, the Dirac delta function in the initial condition (4.6) requires an infinite number of eigenfunctions of y for the series summations in § 3.5 when $t \to 0$. Fortunately, the truncation error will exponentially decrease as time increases (Barton 1984). Note that the real part of the eigenvalue in (3.18) is $(m\pi)^2$. Thus, the series summations in (3.23), (3.25), (C1) converge exponentially (with $\exp[-(m\pi)^2 t]$), and the truncation error diminishes with a large enough m. The results of $N_y = 8$ and $N_y = 10$ are close to the numerical results, as shown in figure 3. Therefore, we use $N_y = 8$ in the following discussions. The linear–log plot (with a logarithmic scale of time) is used to highlight the alignment of curves in the initial short-time period, showing that the current configurations for the analytical and numerical solution procedures are sufficient.

We also compare the result of the Taylor dispersion coefficient ($D_T = \lim_{t\to\infty} \bar{\sigma}^2/(2t)$) with the value obtained by Ding *et al.* (2021, table 2, Trial 1). For $N_y = 8$, the dimensional D_T is $5.38 \times 10^{-9}\mathrm{m}^2\,\mathrm{s}^{-1}$, which is consistent with the theoretical value of $5.39 \times 10^{-9}\mathrm{m}^2\,\mathrm{s}^{-1}$ given by Ding *et al.* (2021), although both values deviate from the experimental result of $4.26 \times 10^{-9}\mathrm{m}^2\,\mathrm{s}^{-1}$.

5. Effect of point-source release

With the auxiliary-time extension method being verified, one can investigate the effects of transport and flow parameters such as frequency, Schmidt number, Womersley number, etc. These basic effects have been discussed in many previous studies (Chatwin 1975; Vedel & Bruus 2012; Ding *et al.* 2021; Singh & Murthy 2023). In this study, our focus is the effects of the point-source release and the phase shift of velocity (see § 6) on the transport characteristics (especially the higher-order moments including skewness and kurtosis), which can also highlight the tractability of the auxiliary-time extension method.

In this section, we show the generality of the solution procedure by considering different initial conditions. The generality derives from Barton's general solution expressions (Barton 1983) because they are based on an arbitrary initial condition and thus have wide applicability. We consider the same oscillatory Couette flow and parameters as in § 4.2 (see table 1). Both the point-source release ($C_{ini} = \delta(y - y_0)$) and the uniform release ($C_{ini} = 1$) are considered. For the point-source case, three different initial positions $y_0 = 0$, $y_0 = 0.5$ and $y_0 = 1$ are considered.

First, we discuss the effect of point-source release position on the first-order moment of the mean concentration distribution, as shown in figure 4(a, b). Obviously, the mean position of the solute cloud is strongly affected by the initial condition, while the effective drift velocity is weakly affected. Because the absolute value of the velocity at the upper wall is larger than that near the bottom wall, the effective drift velocity of the case with $y_0 = 1$ is larger than that of the case with $y_0 = 0$. The curves of u_d quickly overlap with each other after a short time (approximately half a period). Note that u_d of the case with $y_0 = 0.5$ and the case with a transversely uniform release are nearly the same. This is because the Womersley number is so small that the velocity profile is nearly linear along the transverse direction, as shown in figure 2. Here, u_d is the solute-weighted average velocity. The transport problem with a line-source release is nearly symmetric with respect to the centreline of the channel. Thus, its u_d is nearly equal to the velocity value at the centreline, which is similar to the point-source case with $y_0 = 0.5$.

https://doi.org/10.1017/jfm.2026.11292 Published online by Cambridge University Press

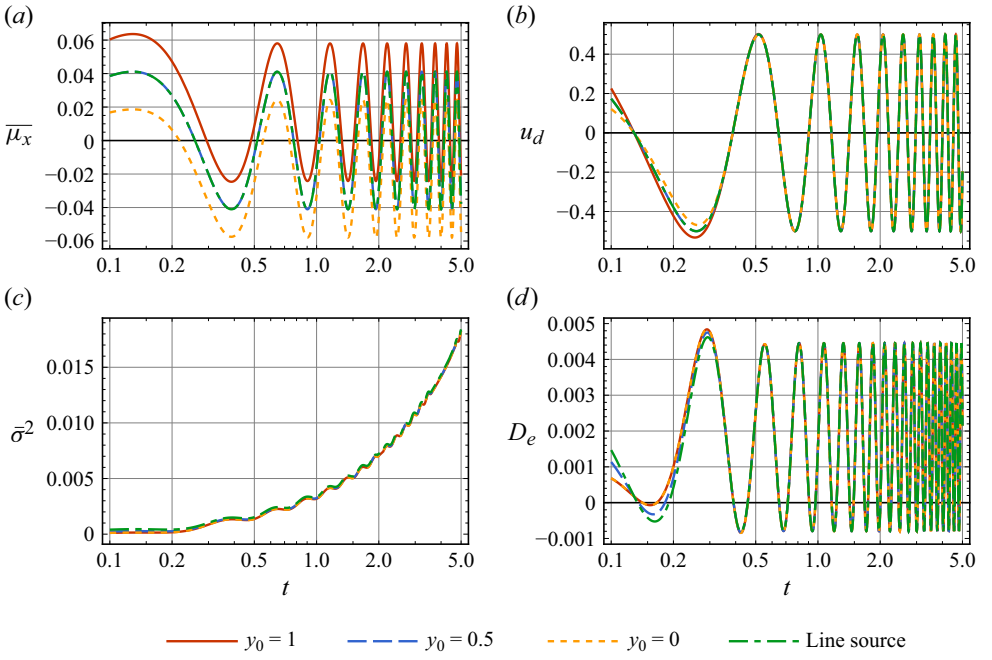


Figure 4. Temporal evolution of (*a*) the mean longitudinal position, (*b*) the effective drift velocity, (*c*) the variance of mean concentration distribution and (*d*) the effective diffusion coefficient for different initial conditions. y_0 is the release position of the point-source release while 'Line source' denotes the uniform release. The parameters are listed in table 1.

For the second-order concentration moment, the temporal evolution of the variance of $\bar{C}$ and the effective diffusion coefficient is shown in figure 4(*c, d*). There is no doubt that the source-release form will affect these characteristics in the initial stage (Vedel *et al.* 2014). Similar to the effective drift velocity, D_e of all the cases are nearly the same after a short time because the angular frequency ω is large. Note that D_e of the case with $y_0 = 0$ is nearly the same as that of the case with $y_0 = 1$. This is because of the quasi-linear velocity profile (with a small *Wo*). The spread of the solute cloud relative to the mean position is nearly symmetric for these two cases (or imagine the opposite case with an oscillating bottom wall instead of the upper wall). In addition, it is well known that D_e can be negative in the transport problem with oscillatory flows (Chatwin 1975; Smith 1982*a*; Yasuda 1984), which can also be observed in figure 4(*d*). For the variance, all the curves are rising and are nearly overlapped with each other as t increases.

The results for the higher-order moments of $\bar{C}$, skewness and kurtosis, are shown in figure 5. Similar to the case with a steady flow, both the skewness and kurtosis of the oscillatory case will still approach zero as t increases because the Taylor dispersion regime is reached and $\bar{C}$ becomes Gaussian. As pointed out by Ding *et al.* (2021, (28)), the decay rate of *Sk* for this single-frequency flow is $t^{-3/2}$, faster than the steady case ($t^{-1/2}$). However, when the flow has a non-zero net flow rate, the decay rate can be in the same order as the steady case. Moreover, the temporal evolution of skewness and kurtosis will be strongly affected by the initial condition.

For skewness, the point-source case with $y_0 = 0.5$ and the line-source case have a nearly zero value of *Sk*, which means that $\bar{C}$ is nearly symmetric with respect to the mean position of the solute cloud. This is because the velocity profile is nearly linear along the transverse direction because the Womersley number is so small (see figure 2).

https://doi.org/10.1017/jfm.2026.11292 Published online by Cambridge University Press

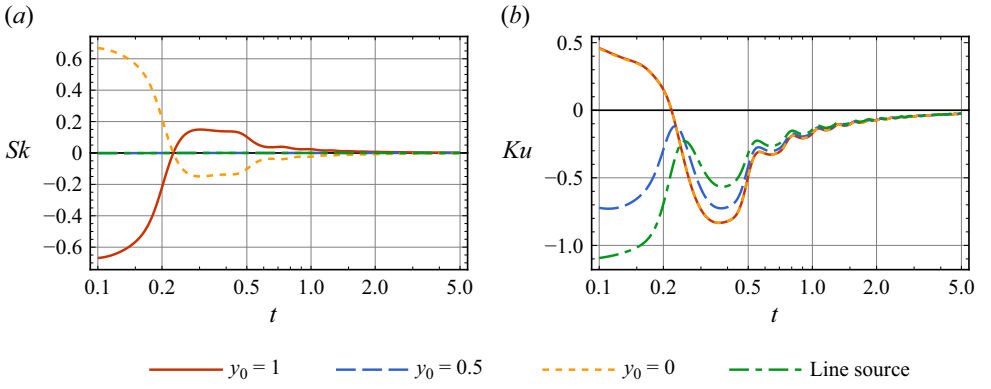


Figure 5. Temporal evolution of (*a*) skewness and (*b*) kurtosis of the mean concentration distribution for different initial conditions. y_0 is the release position of the point-source release while 'Line source' denotes the uniform release. Other parameters are listed in table 1.

As discussed for figure 4, the whole transport problem is quasi-symmetric with respect to the vertical line $x = 0$. Compared with the non-zero kurtosis in figure 5(*b*), a nearly zero *Sk* in the initial stage cannot ensure the Gaussianity of the concentration distribution. The Taylor dispersivity is neither enhanced nor inhibited because the flow configuration is unchanged. Skewness can be strongly affected by the initial condition.

For the point-source cases with $y_0 = 0$ and $y_0 = 1$, their skewness values are nearly equal in magnitude but opposite in sign due to the quasi-symmetry of this specific transport problem. A positive *Sk* means that the distribution is upstream-leaning and *vice versa*. Note that the sign of skewness can be changed during the transport process due to the oscillation of the velocity profile.

The transient evolution of kurtosis is much more complicated, although the oscillation induced by the flow is not apparent. For the point-source cases with $y_0 = 0$ and $y_0 = 1$, their kurtosis curves nearly overlap with each other due to the quasi-symmetry of this specific transport problem with a small *Wo*. When the time is small, the tailedness is larger than the Gaussian distribution (positive *Ku*, leptokurtic). However, the sign of kurtosis is changed during the transport process due to the velocity oscillation. For the other two cases, the absolute value of kurtosis of the line-source case is larger than that of a point source with $y_0 = 0.5$. However, this trend can be reversed as time increases.

6. Effect of phase shift of velocity profile

Another benefit of the auxiliary-time extension method is that it can easily deal with the phase shift effect of the velocity field on the transport characteristics. Ding *et al.* (2021) have discussed this effect on skewness's sign change, with the transversely uniform release. Here, we further investigate the effect and show the result of other characteristics.

6.1. *Solution procedure to address phase shift*

First, we follow Ding *et al.* (2021) and add a phase shift s in the oscillatory velocity field as

$$u_s(y, t) \triangleq u(y, t + s). \tag{6.1}$$

Then, replace the original velocity field u in (2.1*a*) with the shifted velocity field u_s.

https://doi.org/10.1017/jfm.2026.11292 Published online by Cambridge University Press

Typically, one needs to re-solve the whole problem of the concentration moments to impose the phase shift. However, with the auxiliary-time extension method, we can directly obtain the solution with a simple transformation of the time variable t_1. Notice that t_1 is imposed in (3.1) as $t_1 = \omega t$. To address the phase shift, we impose the following time variables instead:

$$t_0 = t, \quad t_{1s} = \omega(t + s). \tag{6.2}$$

Notice that $t_{1s} = t_1 + \omega s$. Then, similar to (3.2), we define u_{s1} to replace the oscillatory velocity field for the shifted two-time-variable system and

$$\begin{aligned} u_{s1}(y, t_{1s}) &\triangleq u_s(y, t) = u(y, t + s) \\ &= u\left(y, \frac{t_{1s}}{\omega} - s + s\right) = u\left(y, \frac{t_{1s}}{\omega}\right) \\ &= u_1\left(y, t_{1s}\right). \end{aligned} \tag{6.3}$$

Namely, the function u_{s1} is in the same form as u_1. Thus, the governing equation for the shifted two-time-variable system is the same as that of the original system in (3.6).

To sum up, there is no need to re-solve the whole problem for the phase shift in flow velocity. The solution of the moments for the shifted two-time-variable system can be obtained by replacing t_1 with t_{1s} in the solution of the original two-time-variable system given in § 3.5. Namely,

$$P_{sn}(y, t_0, t_{1s}) = P_n(y, t_0, t_{1s}), \tag{6.4}$$

where P_{sn} is the nth-order moment of the shifted two-time-variable system. Based on (3.14), the nth-order concentration moments C_{sn} of the shifted problem is

$$C_{sn}(y, t) = P_{sn}(y, t_0, t_{1s}) = P_n(y, t, \omega(t + s)). \tag{6.5}$$

Note that one could not obtain $C_{sn}(y, t)$ through $C_n(y, t)$ by simply replacing t with $t + s$. Fortunately, this could be done by P_n with t_1 replaced by $t_1 + \omega s$, which can be considered as a benefit of the auxiliary-time extension method. In addition, as discussed by Ding (2025), the decay rate to the Taylor dispersion regime can be characterised by the non-zero eigenvalue with the smallest real part, $1/\mathrm{Re}(\lambda)$. Replacing t_1 would not influence the eigenvalue (3.18). Therefore, the decay rate to the Taylor dispersion regime is not affected by the phase shift.

We also perform the numerical verification for the phase shift effect, as shown in figure 11. The analytical result by (6.5) agrees well with the numerical result.

6.2. *Results of transport characteristics*

To illustrate the effect of the phase shift on the transport characteristics, we consider the same oscillatory velocity profile as that in previous sections, but with different phase shift $s = 0, \pi/4, \pi, \pi/2, 3\pi/4$. A point-source release is considered ($y_0 = 1$). Note that the case with $s = \pi$ is the reverse case of the case with $s = 0$, due to the symmetry of the transport problem. Thus, only four cases are considered.

For the first-order moment of $\bar{C}$ and the effective drift, it can be seen in figure 6(*a, b*) that the effect of the phase shift is remarkable. Note that the effective drift is the solute-weighted average velocity, while the overall transverse distribution is not affected by the velocity field. Thus, the phase shift of the velocity will directly be reflected in the effective drift. It then leads to the accumulative change in the mean position of the solute cloud as time increases.

https://doi.org/10.1017/jfm.2026.11292 Published online by Cambridge University Press

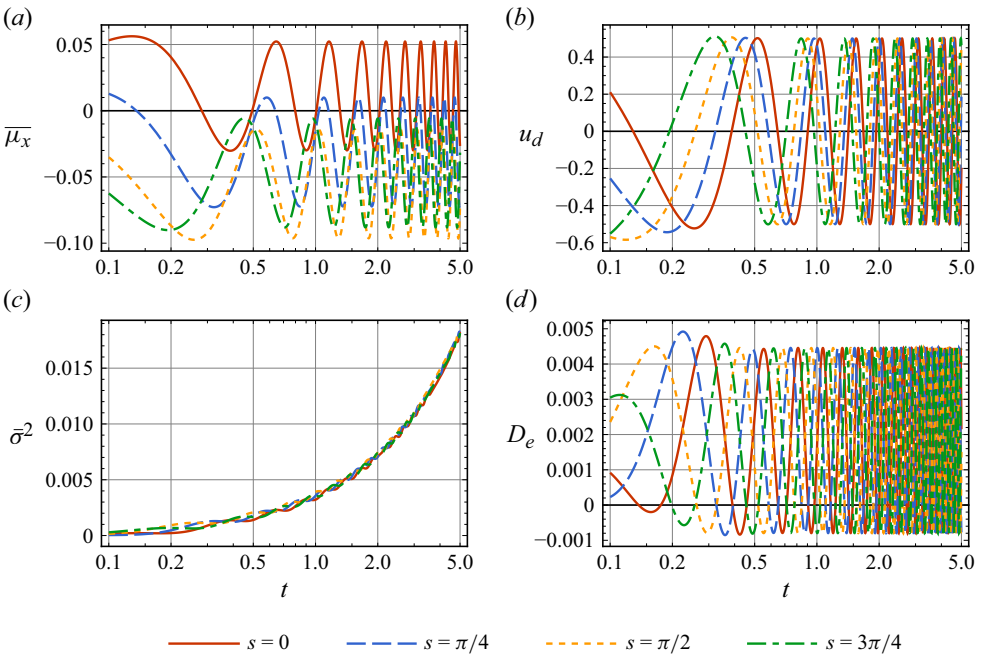


Figure 6. Temporal evolution of (*a*) the mean longitudinal position, (*b*) the effective drift velocity, (*c*) the variance of mean concentration distribution and (*d*) the effective diffusion coefficient for different phase shift s. The initial condition is a point-source release at $y_0 = 1$. Other parameters are listed in table 1.

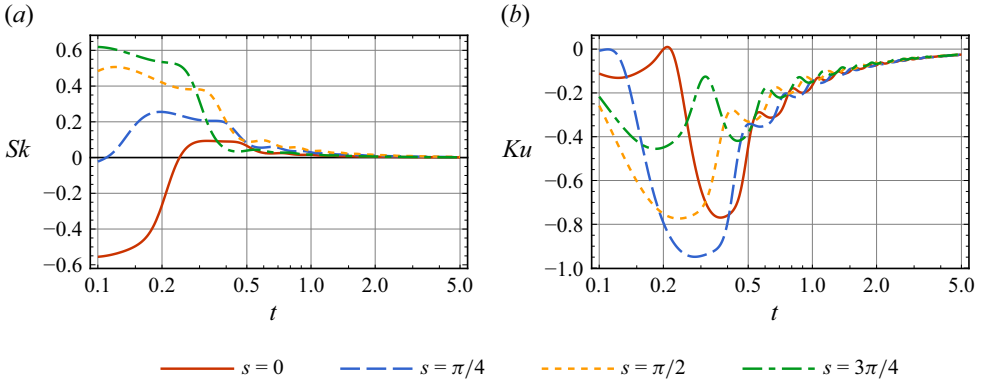


Figure 7. Temporal evolution of (*a*) skewness and (*b*) kurtosis of the mean concentration distribution for different phase shift s. The initial condition is a point-source release at $y_0 = 1$. Other parameters are listed in table 1.

Figure 6(*c*, *d*) shows the phase shift effect on the variance of $\bar{C}$ and the effective diffusion coefficient. Note that D_e is initially zero because of the instantaneous release. The phase shift will change the time when D_e reaches its maximum value. Then, D_e will decay to the oscillatory state and reach the Taylor dispersion regime. For the variance, similar to the effect of the initial condition discussed in § 5, the accumulative influence of the phase shift is weak and all the curves are nearly close to each other as t increases.

As discussed by Ding *et al.* (2021), the phase shift can change the sign of skewness, which is clearly observed in figure 7(*a*). Unlike the line-source case of Ding *et al.* (2021), the point-source case discussed here has a large non-zero skewness in the initial stage of

https://doi.org/10.1017/jfm.2026.11292 Published online by Cambridge University Press

the transport process. Thus, the oscillation of skewness is not apparent. However, the phase shift of the velocity field can still make a qualitative change in the asymmetry of the mean concentration distribution. If we compare the cases with $s = 0$ and $s = \pi$ (not shown here), then the curves will be flipped with respect to the t-axis due to the symmetric property of the transport problem.

For kurtosis, the phase shift will change the sign of Ku, as shown in figure 7(b). The phase shift of the velocity field can be transferred to kurtosis, as the oscillation of Ku is apparent during the initial stage of the transport process. For the four considered cases, the temporal evolution curves have many intersections with each other even in the first period, showing the phase shift effect is complex.

7. Conclusions

Understanding the transient dispersion in oscillatory flows is crucial for many practical applications. The method of concentration moments is a powerful analytical tool for analysing the transport characteristics and has been well developed for the transport problems in steady flows. Barton (1983) has provided the general solution expressions for the first-few-order moments, using separation of variables. However, for unsteady flows, these results cannot be applied directly.

Many previous studies (Mukherjee & Mazumder 1988; Vedel & Bruus 2012) had to use the moment method from the very beginning: re-solving the governing equation of moments. However, due to the complication induced by the time-periodic velocity field, the solution procedure is not as straightforward and general as that by Barton (1983). For higher-order statistics, the skewness has been derived only for a specific initial condition (Ding *et al.* 2021), while the solution for kurtosis remains analytically intractable, necessitating the use of numerical methods (Singh & Murthy 2023).

This manuscript proposes a novel analytical procedure by the introduction of an auxiliary oscillation time variable for the inherent oscillatory characteristics of the dispersion and extends the original transport problem to a two-time-variable problem, with the new time dimension virtually viewed as an additional 'transverse' space. Then, there is no need to re-solve the moment equation: the general solution expressions by Barton (1983) now can be used directly because the flow velocity becomes 'steady' after splitting the time variable. We remark that although the introduction of the time variables bears structural similarities to the two-time-scale homogenisation method, these two methods are fundamentally distinct in their underlying principles. The present method does not rely on either a small perturbation parameter or scale-separation analysis. The objective here is the concentration moments, not the long-time asymptotic concentration distribution (as in the homogenisation method).

The solution procedure for concentration moments is then greatly simplified to only two steps: (i) identifying the eigenvalue problem and (ii) substituting the eigenvalues and eigenfunctions in Barton's expressions. This auxiliary-time extension treatment not only offers an intuitive physical perspective for the velocity oscillation, but also clarifies the solution structure of concentration moments. The complications encountered in previous studies can be avoided, making it feasible to investigate the temporal evolution of higher-order statistics and more applicable for complex transport problems in oscillatory flows. For example, this method has been extended to investigate the dispersion of swimming microorganisms in oscillatory channel flows (Wang *et al.* 2025). The active dispersion phenomenon is of growing research interest (Peng 2024; Caldag & Bees 2025; Fung, Caldag & Bees 2025; Zeng *et al.* 2025*a*). Future work can extend this method to oscillatory pipe flows and three-dimensional channel flows by changing the eigenfunction framework according to the cross-section geometry.

https://doi.org/10.1017/jfm.2026.11292 Published online by Cambridge University Press

As a preliminary verification, we examine the transport problem in an oscillatory Couette flow. The numerical results by the Brownian dynamics simulation method are used for comparison and show good agreement with the analytical solutions by the auxiliary-time extension method.

Furthermore, to highlight the tractability of the auxiliary-time extension method, we investigate the effects of the point-source release and the phase shift of velocity on the transport characteristics, especially on higher-order statistics like skewness and kurtosis. The generality of the solution procedure derives from Barton's general solution expressions for arbitrary initial conditions. For the phase shift of velocity, a simple transformation of the newly introduced time variable can be used to handle the phase shift effect without re-solving the moment equation. The oscillation of skewness is not apparent in the case with a point-source release. The phase shift of the velocity field can be remarkably transferred to the temporal evolution of kurtosis. Both these two effects can change the sign of skewness and kurtosis, qualitatively affecting the asymmetry and the tailedness of the mean concentration distribution.

Acknowledgements. The authors would like to thank Dr Bohan Wang for constructive discussions.

Funding. This work is supported by the Science and Technology Development Fund (FDCT) of Macao SAR (Project Nos. 0025/2024/RIA1, 0018/2023/ITP1, 0031/2024/AMJ and 0001/2024/NRP) and the National Natural Science Foundation of China (Grant No. 52079001).

Declaration of interests. The authors report no conflict of interest.

Appendix A. Governing equations of moments

To derive the governing equation of concentration moments, it is assumed that concentration decays exponentially (Aris 1956; Li *et al.* 2017). Integrating (2.1*a*), according to the definition of C_n in (2.5), and using the integration by parts formula, we have

$$\frac{\partial C_n}{\partial t} - \frac{\partial^2 C_n}{\partial y^2} = n\, u(y,t) C_{n-1} + \frac{n(n-1)}{Pe^2} C_{n-2} \tag{A1}$$

for $n = 0, 1, 2, \ldots$. Notice that $C_{-1} = C_{-2} = 0$ are auxiliary terms. The boundary conditions of C_n are the same as that of C in (2.1*b*):

$$\left.\frac{\partial C_n}{\partial y}\right|_{y=0} = \left.\frac{\partial C_n}{\partial y}\right|_{y=1} = 0. \tag{A2}$$

For the initial condition, according to (2.1*c*), we have

$$C_n|_{t=0} = \begin{cases} C_{ini}(y), & n = 0, \\ 0, & n = 1, 2, \ldots. \end{cases} \tag{A3}$$

Note that the governing equation (A1) of C_n contains the time-dependent velocity field $u(y,t)$ as a source term on the left side. Thus, obtaining time-integral solutions for C_n is more complicated compared with steady flow cases, particularly for higher-order moments.

Appendix B. Solution of the eigenvalue problem

For the eigenvalue problem (3.16), one can use the method of separation of variables to obtain the solution.

https://doi.org/10.1017/jfm.2026.11292 Published online by Cambridge University Press

Assume that the solution form of the eigenfunction f is

$$f(y, t_1) = Y(y)T_1(t_1). \tag{B1}$$

Substituting it into (3.16*a*) yields

$$-\omega\frac{1}{T_1}\frac{\mathrm{d}T_1}{\mathrm{d}t_1} + \frac{1}{Y}\frac{d^2Y}{\mathrm{d}y^2} = -\lambda. \tag{B2}$$

Note that Y depends only on y, T_1 depends only on t_1 and the eigenvalue λ is a constant. Therefore,

$$\frac{1}{Y}\frac{\mathrm{d}^2Y}{\mathrm{d}y^2} = -\lambda + \omega\frac{1}{T_1}\frac{\mathrm{d}T_1}{\mathrm{d}t_1} = -\lambda_y, \tag{B3}$$

where λ_y is a constant. We can also introduce another constant

$$\lambda_{t_1} = \frac{\lambda - \lambda_y}{\omega} \tag{B4}$$

for T_1.

Note that the boundary conditions (3.16*b*), (3.16*c*) are also separable. Thus, for $Y(y)$, we have

$$\frac{\mathrm{d}^2Y}{\mathrm{d}y^2} = -\lambda_y Y, \tag{B5a}$$

$$\left.\frac{\partial Y}{\partial y}\right|_{y=0} = \left.\frac{\partial Y}{\partial y}\right|_{y=1} = 0. \tag{B5b}$$

According to the boundary conditions, the solution of $Y(y)$ is a trigonometric function. We have

$$Y(y) = a_m\cos(m\pi y) + b_m\sin(m\pi y), \quad \lambda_y = (m\pi)^2, \tag{B6}$$

and $m = 0, 1, 2, \ldots$. Here, $b_m = 0$ and a_m is a constant coefficient.

For T_1, we have

$$\frac{\mathrm{d}T_1}{\mathrm{d}t_1} = \lambda_{t_1}T_1, \tag{B7a}$$

$$T_1|_{t_1=0} = T_1|_{t_1=2\pi}. \tag{B7b}$$

Due to the periodic condition (B7*b*), the solution of T_1 is the complex Fourier series. We have

$$T_1 = a_k\exp(\mathrm{i}kt_1), \quad \lambda_{t_1} = \mathrm{i}k, \tag{B8}$$

where $k = 0, \pm1, \pm2, \ldots$ and a_k is the constant coefficient.

Finally, returning to (B1), we obtain

$$f(y, t_1) = a_m\cos(m\pi y)a_k\exp(\mathrm{i}kt_1), \tag{B9}$$

and the corresponding eigenvalue (B4)

$$\lambda = \lambda_y + \omega\lambda_{t_1} = (m\pi)^2 + \mathrm{i}k\omega. \tag{B10}$$

https://doi.org/10.1017/jfm.2026.11292 Published online by Cambridge University Press

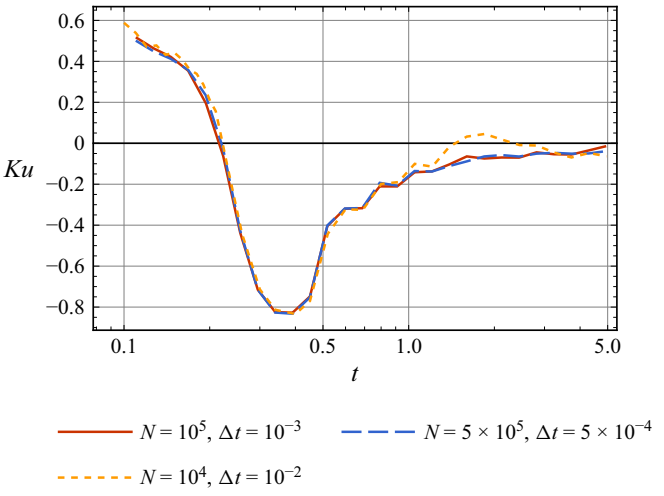


Figure 8. Numerical results of kurtosis of the mean concentrations distribution under different set-up of the number of particles (N) and the time step (Δt). The initial condition is a point-source release at $y_0 = 0.75$. Other parameters are listed in table 1.

Appendix C. Solution of second-order moment

For the second-order moment, based on (2.14) of Barton (1984), the solution is

$$\begin{aligned} P_2(y, t_0, t_1) = &\sum_{i=0}^{\infty} a_i B_{i,i}^2 t_0^2 \mathrm{e}^{-\lambda_i t_0} f_i + \sum_{\substack{i,j=0 \\ j\neq i}}^{\infty} \frac{2E_{i,j}a_j(\mathrm{e}^{-\lambda_j t_0} - \mathrm{e}^{-\lambda_i t_0})}{\lambda_i - \lambda_j} f_i + \sum_{i=0}^{\infty} 2a_i E_{i,i} t_0 \mathrm{e}^{-\lambda_i t_0} f_i \\ &+ \sum_{\substack{i,j,k=0 \\ k\neq j, k\neq i}}^{\infty} \frac{2a_k B_{j,k} B_{i,j}(\mathrm{e}^{-\lambda_k t_0} - \mathrm{e}^{-\lambda_i t_0})}{(\lambda_k - \lambda_i)(\lambda_k - \lambda_j)} f_i + \sum_{\substack{i,j=0 \\ i\neq j}}^{\infty} \frac{2a_i B_{j,i} B_{i,j} t_0 \mathrm{e}^{-\lambda_i t_0}}{\lambda_j - \lambda_i} f_i \\ &+ \sum_{\substack{i,j,k=0 \\ k\neq j, j\neq i}}^{\infty} \frac{2a_k B_{j,k} B_{i,j}(\mathrm{e}^{-\lambda_j t_0} - \mathrm{e}^{-\lambda_i t_0})}{(\lambda_k - \lambda_j)(\lambda_i - \lambda_j)} f_i + \sum_{\substack{i,k=0 \\ k\neq i}}^{\infty} \frac{2a_k B_{i,k} B_{i,i} t_0 \mathrm{e}^{-\lambda_i t_0}}{\lambda_k - \lambda_i} f_i \\ &+ \sum_{\substack{i,j=0 \\ j\neq i}}^{\infty} \frac{2a_j B_{j,j} B_{i,j}\left[\mathrm{e}^{-\lambda_i t_0} - \mathrm{e}^{-\lambda_j t_0} + (\lambda_i - \lambda_j) t_0 \mathrm{e}^{-\lambda_j t_0}\right]}{(\lambda_j - \lambda_i)^2} f_i, \end{aligned} \tag{C1}$$

where $E_{i,j}$ is the coefficient related to the diffusion coefficient D,

$$\begin{aligned} E_{i,j} &\triangleq \langle f_i, Df_j \rangle \\ &= \int_0^{2\pi} \int_0^1 f_i^\star(y, t_1) D f_j(y, t_1)\, \mathrm{d}y\, \mathrm{d}t_1 \\ &= D\delta_{ij} \end{aligned} \tag{C2}$$

for $i, j = 0, 1, \ldots$. Note that $D = 1/Pe^2$ for the transport problem considered in (3.6).

For the third- and fourth-order moments, the readers can refer to (3.17) of Barton (1983), an analytical expression of the third-order moment can also be found in Appendix A of Yang *et al.* (2021). Their expressions are too long to be reproduced here. For practical purposes, readers can refer to the study of Jiang *et al.* (2022), with a Mathematica notebook provided at https://doi.org/10.5281/zenodo.14927459.

https://doi.org/10.1017/jfm.2026.11292 Published online by Cambridge University Press

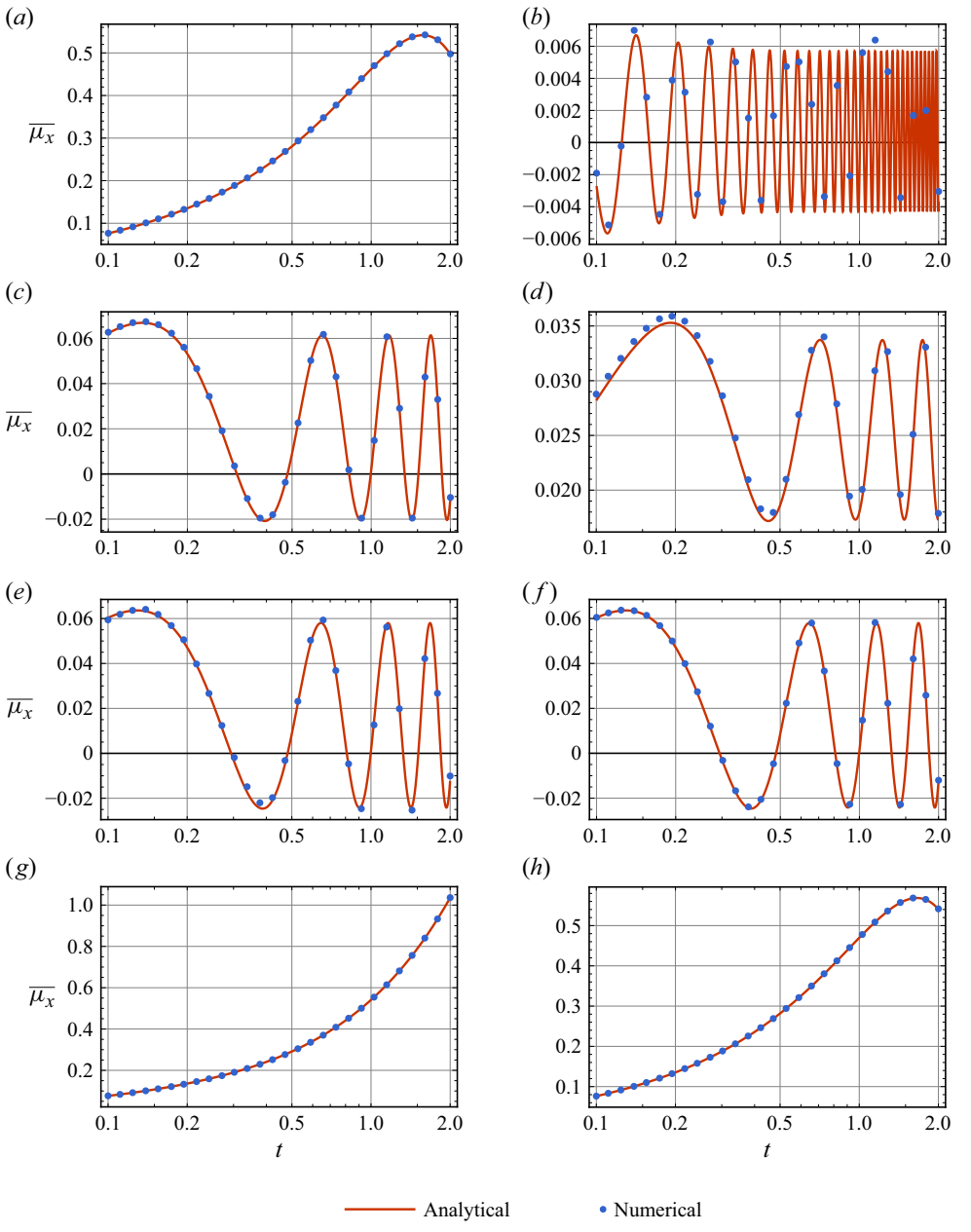


Figure 9. More comparisons between the analytical and numerical results under different parameter set-ups. The first-order moment of mean concentration distribution ($\bar{\mu}_x$) is shown. The initial condition is a point-source release at $y_0 = 0.75$. With fixed parameters listed in table 1, the modified parameter in each case is: (*a*) $\omega = 1$; (*b*) $\omega = 100$; (*c*) $Wo = 1$; (*d*) $Wo = 10$; (*e*) $Pe = 1$; (*f*) $Pe = 10$; (*g*) $Sc = 10$; and (*h*) $Sc = 100$.

Appendix D. Numerical stochastic differential equations

D.1. Euler–Maruyama scheme

We use the Euler–Maruyama scheme to solve the SDEs (4.5). Let X_n and Y_n denote the position of a particle at the nth time step $t_n = n\Delta t$. We have

https://doi.org/10.1017/jfm.2026.11292 Published online by Cambridge University Press

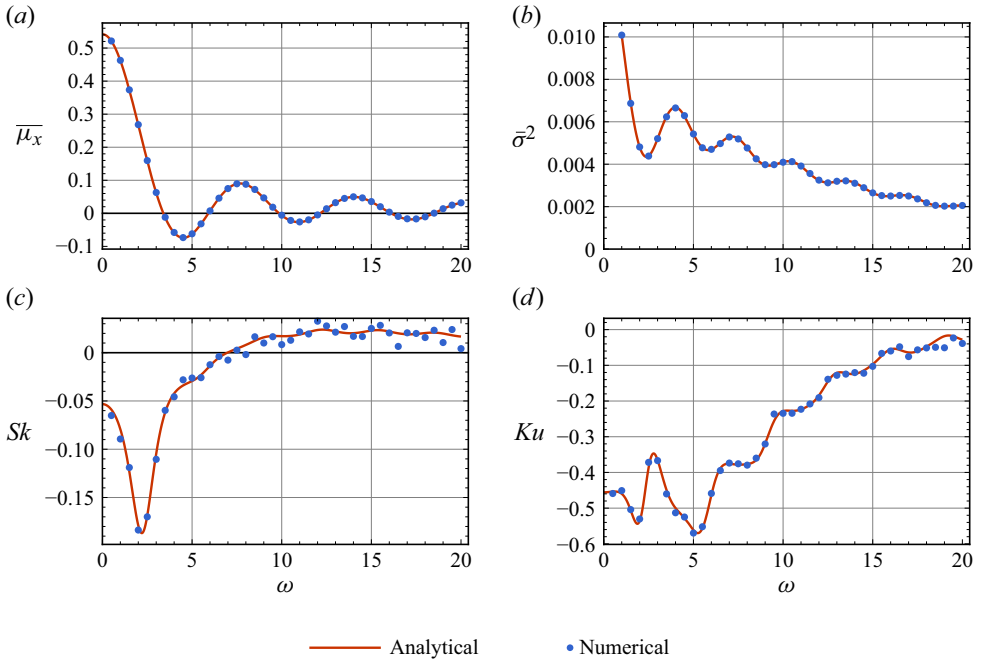


Figure 10. Comparisons between the analytical and numerical results for different angular frequency ω at $t = 1$: (*a*) the first-order moment of mean concentration distribution; (*b*) the variance of $\bar{C}$; (*c*) the skewness of $\bar{C}$; and (*d*) the kurtosis of $\bar{C}$. The initial condition is a point-source release at $y_0 = 0.75$. Other parameters are listed in table 1. Note that *Wo* is fixed.

$$X_{n+1} = X_n + u(Y_n, t_n)\Delta t + \frac{\sqrt{2\Delta t}}{Pe}\Delta W_1, \tag{D1a}$$

$$Y_{n+1} = Y_n + \sqrt{2\Delta t}\,\Delta W_2, \tag{D1b}$$

where ΔW_1 and ΔW_2 are random variables generated at each time step. They satisfy the standard normal distribution, i.e. $\Delta W_1 \sim \mathrm{N}(0, 1)$ and $\Delta W_2 \sim \mathrm{N}(0, 1)$. Here, N denotes the normal distribution. In our code, we add $t_{n+1} = t_n + \Delta t$ to (D1) such that the whole system is autonomous.

On the channel walls ($y = 0$ and $y = 1$), the specular reflection model (billiard-like reflection) is adopted to simulate the non-penetration boundary condition (2.1*b*). If a particle exceeds the boundaries after the calculation at the $n + 1$ time step, it is reflected back to the channel:

$$Y_{n+1} \to -Y_{n+1} \quad \text{if } Y_{n+1} < 0, \tag{D2a}$$

$$Y_{n+1} \to 2 - Y_{n+1} \quad \text{if } Y_{n+1} > 1. \tag{D2b}$$

For the initial condition, we set $X_0 = 0$ and $Y_0 = 1$ for a point-source release at $y_0 = 1$. For the uniform release ($C_{ini} = 1$), X_0 is a random variable generated from the uniform distribution on the interval [0, 1].

The numerical error of the Euler–Maruyama scheme is mainly determined by the time step Δt (which scales as $\mathcal{O}(\sqrt{\Delta t})$) and the number of particles N. In figure 8, we have compared the numerical results of kurtosis with different Δt and N. The curves of the result of $N = 10^5$ and $\Delta t = 10^{-3}$ are nearly overlapped with the result of $N = 5 \times 10^5$ and $\Delta t = 5 \times 10^{-2}$, which means that the numerical independence had been achieved

https://doi.org/10.1017/jfm.2026.11292 Published online by Cambridge University Press

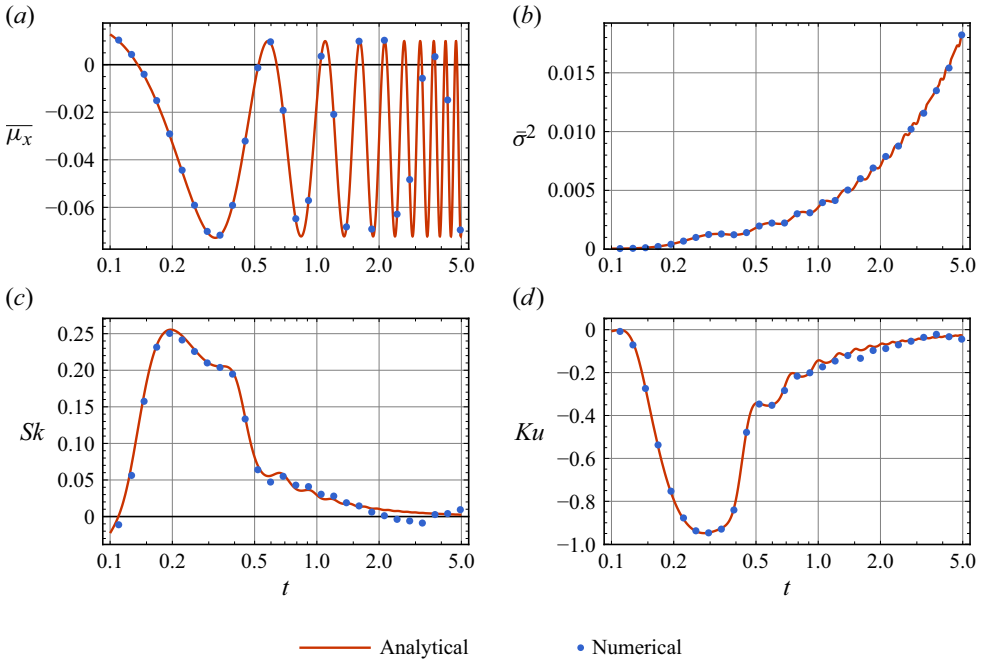


Figure 11. Comparison between the analytical solution of concentration moments and the numerical result for the phase shift effect: (*a*) the first-order moment of mean concentration distribution; (*b*) the variance of $\bar{C}$; (*c*) the skewness of $\bar{C}$; and (*d*) the kurtosis of $\bar{C}$. The initial condition is a point-source release at $y_0 = 0.75$. Other parameters are listed in table 1.

at this set-up. The result of $N = 10^4$ and $\Delta t = 10^{-2}$ considerably deviates from the other two when t is large, which means that the time step is too coarse. Therefore, we use $N = 10^5$ and $\Delta t = 10^{-3}$ for the numerical simulations. Python code is provided at https://doi.org/10.5281/zenodo.16781949.

D.2. Comparisons under different parameter setups

In figure 3, we compare the analytical and numerical results under one single parameter set-up. Some parameters used in the comparison (listed in table 1) are small. The proposed two-time-variable method does not require any small parameters or scale-separation conditions as the two-scale homogenisation method does. To demonstrate this point more clearly, we compare the results under different parameter set-ups in figure 9. We take the first-order moment of mean concentration distribution as an example. Both the analytical results of the cases with a smaller angular frequency and with a much larger angular frequency agree well with the numerical results. The cases with different magnitude values of *Pe*, *Wo* and *Sc* are also consistent across the analytical and numerical results.

The comparison under a continuous change of parameters is shown in figure 10. Because the angular frequency ω can be considered as a distinctive parameter for oscillatory flows compared with the steady case, we choose ω for the comparison. Moreover, only the results at $t = 1$ are plotted for a more direct comparison.

Figure 10 shows the curves of the basic dispersion characteristics as ω increases, which can be considered as a local sensitivity of ω. The analytical results agree well with the numerical ones by random walk simulations. Moreover, there is an overall decreasing trend of the variance in figure 10(*b*). Note that the Womersley number *Wo* is fixed in the comparison (and thus the Schmidt number *Sc* changes as ω varies), namely, the spatial

https://doi.org/10.1017/jfm.2026.11292 Published online by Cambridge University Press

shape of the Stokes layer remains unchanged. The oscillation can inhibit the dispersion process. This has been investigated by Ding *et al.* (2021, figure 2): the Taylor dispersivity decreases as ω increases when *Wo* is fixed.

D.3. Phase shift

We also perform the numerical simulation for the case with a phase shift of the velocity field. Figure 11 shows the numerical verification for the treatment of the phase shift effect presented in § 6.1. The analytical solutions of the transport characteristics agree well with the numerical results.

References

Allen, C.M. 1982 Numerical simulation of contaminant dispersion in estuary flows. *Proc. R. Soc. Lond. A* **381** (1780), 179–194.

Aminian, M., Bernardi, F., Camassa, R., Harris, D.M. & McLaughlin, R.M. 2016 How boundaries shape chemical delivery in microfluidics. *Science* **354** (6317), 1252–1256.

Aminian, M., Bernardi, F., Camassa, R. & McLaughlin, R.M. 2015 Squaring the circle: geometric skewness and symmetry breaking for passive scalar transport in ducts and pipes. *Phys. Rev. Lett.* **115** (15), 154503.

Andersson, B. & Berglin, T. 1981 Dispersion in laminar flow through a circular tube. *Proc. R. Soc. Lond. A* **377** (1770), 251–268.

Aquino, T. 2024 Equilibrium distributions under advection–diffusion in laminar channel flow with partially absorbing boundaries. *J. Fluid Mech.* **985**, A16.

Aris, R. 1956 On the dispersion of a solute in a fluid flowing through a tube. *Proc. R. Soc. Lond. A* **235** (1200), 67–77.

Aris, R. 1960 On the dispersion of a solute in pulsating flow through a tube. *Proc. R. Soc. Lond. A* **259** (1298), 370–376.

Attinger, S., Dentz, M., Kinzelbach, H. & Kinzelbach, W. 1999 Temporal behaviour of a solute cloud in a chemically heterogeneous porous medium. *J. Fluid Mech.* **386**, 77–104.

Bandyopadhyay, S. & Mazumder, B.S. 1999 Unsteady convective diffusion in a pulsatile flow through a channel. *Acta Mechanica* **134** (1–2), 1–16.

Barik, S. & Dalal, D.C. 2019 Multi-scale analysis for concentration distribution in an oscillatory Couette flow. *Proc. R. Soc. Lond. A* **475** (2221), 20180483.

Barton, N.G. 1983 On the method of moments for solute dispersion. *J. Fluid Mech.* **126**, 205–218.

Barton, N.G. 1984 An asymptotic theory for dispersion of reactive contaminants in parallel flow. *J. Austral. Math. Soc. Ser. B Appl. Maths* **25** (3), 287–310.

Berkowitz, B., Cortis, A., Dentz, M. & Scher, H. 2006 Modeling non-Fickian transport in geological formations as a continuous time random walk. *Rev. Geophys.* **44** (2), RG2003.

Bowden, K.F. 1965 Horizontal mixing in the sea due to a shearing current. *J. Fluid Mech.* **21** (1), 83–95.

Brenner, H. & Edwards, D.A. 1993 *Macrotransport Processes*. Butterworth-Heinemann.

Caldag, H.O. & Bees, M.A. 2025 Fine-tuning the dispersion of active suspensions with oscillatory flows. *Phil. Trans. R. Soc. Math. Phys. Engng Sci.* **383** (2304), 20240259.

Camassa, R., Lin, Z. & McLaughlin, R.M. 2010 The exact evolution of the scalar variance in pipe and channel flow. *Commun. Math. Sci.* **8** (2), 601–626.

Chatwin, P.C. 1970 The approach to normality of the concentration distribution of a solute in a solvent flowing along a straight pipe. *J. Fluid Mech.* **43** (2), 321–352.

Chatwin, P.C. 1972 The cumulants of the distribution of concentration of a solute dispersing in solvent flowing through a tube. *J. Fluid Mech.* **51** (1), 63–67.

Chatwin, P.C. 1975 On the longitudinal dispersion of passive contaminant in oscillatory flows in tubes. *J. Fluid Mech.* **71** (3), 513–527.

Chu, H.C.W., Garoff, S., Przybycien, T.M., Tilton, R.D. & Khair, A.S. 2019 Dispersion in steady and time-oscillatory two-dimensional flows through a parallel-plate channel. *Phys. Fluids* **31** (2), 022007.

Das, D., Dhar, S., Kairi, R.R., Mondal, K.K. & Poddar, N. 2024*a* Analysis of environmental transport of suspended sediment particles in a tidal wetland flow under the effect of floating vegetation absorption. *Commun. Nonlinear Sci. Numer. Simul.* **132**, 107888.

Das, D., Mondal, K.K., Poddar, N. & Wang, P. 2024*b* Transient dispersion of a reactive solute in an oscillatory Couette flow through an anisotropic porous medium. *Phys. Fluids* **36** (2), 023610.

https://doi.org/10.1017/jfm.2026.11292 Published online by Cambridge University Press

DEBNATH, S., SAHA, A.K., MAZUMDER, B.S. & ROY, A.K. 2019 Transport of a reactive solute in a pulsatile non-Newtonian liquid flowing through an annular pipe. *J. Engng Maths* **116** (1), 1–22.
DENTZ, M. & CARRERA, J. 2003 Effective dispersion in temporally fluctuating flow through a heterogeneous medium. *Phys. Rev. E* **68** (3), 036310.
DENTZ, M. & CARRERA, J. 2005 Effective solute transport in temporally fluctuating flow through heterogeneous media. *Water Resour. Res.* **41** (8), W08414.
DHAR, S., DAS, D., PODDAR, N. & MONDAL, K.K. 2022 Dispersion of fine settling particles in a tidal wetland flow. *J. Hydrol.* **615**, 128701.
DING, L. 2023 Shear dispersion of multispecies electrolyte solutions in the channel domain. *J. Fluid Mech.* **970**, A27.
DING, L. 2025 Long-time asymptotics of passive scalar transport in periodically modulated channels. *J. Fluid Mech.* **1023**, A19.
DING, L., HUNT, R., MCLAUGHLIN, R.M. & WOODIE, H. 2021 Enhanced diffusivity and skewness of a diffusing tracer in the presence of an oscillating wall. *Res. Math. Sci.* **8** (3), 34.
DRAZIN, P.G. & RILEY, N. 2006 *The Navier–Stokes Equations: A Classification of Flows and Exact Solutions*. Cambridge University Press.
ELHANATI, D., DROR, I. & BERKOWITZ, B. 2023 Impact of time-dependent velocity fields on the continuum-scale transport of conservative chemicals. *Water Resour. Res.* **59** (9), e2023WR035266.
FIFE, P.C. & NICHOLES, K.R.K. 1975 Dispersion in flow through small tubes. *Proc. R. Soc. Lond. A* **344** (1636), 131–145.
FISCHER, H. 1972 Mass transport mechanisms in partially stratified estuaries. *J. Fluid Mech.* **53** (4), 671–687.
FRANKEL, I. & BRENNER, H. 1991 Generalized Taylor dispersion phenomena in unbounded homogeneous shear flows. *J. Fluid Mech.* **230**, 147–181.
FUNG, L., CALDAG, H.O. & BEES, M. 2025 Foundation and challenges in modelling dilute active suspensions. *Phil. Trans. R. Soc. Math. Phys. Engng Sci.* **383** (2304), 20240251.
GAVER, D.P. & GROTBERG, J.B. 1990 The dynamics of a localized surfactant on a thin film. *J. Fluid Mech.* **213**, 127–148.
GILL, W.N. & SANKARASUBRAMANIAN, R. 1971 Dispersion of a non-uniform slug in time-dependent flow. *Proc. R. Soc. Lond. A* **322** (1548), 101–117.
GROTBERG, J.B. & JENSEN, O.E. 2004 Biofluid mechanics in flexible tubes. *Annu. Rev. Fluid Mech.* **36**, 121–147.
GROTBERG, J.B., SHETH, B.V. & MOCKROS, L.F. 1990 An analysis of pollutant gas transport and absorption in pulmonary airways. *J. Biomech. Engng* **112** (2), 168–176.
GUAN, M. & CHEN, G. 2024 Streamwise dispersion of soluble matter in solvent flowing through a tube. *J. Fluid Mech.* **980**, A33.
GUAN, M.Y., ZENG, L., LI, C.F., GUO, X.L., WU, Y.H. & WANG, P. 2021 Transport model of active particles in a tidal wetland flow. *J. Hydrol.* **593**, 125812.
GUO, J., JIANG, W., CHEN, G., LI, Z., ALHARBI, N.S. & WAKEEL, M. 2022 Solute dispersion in an open channel turbulent flow: solution by a generalized model. *J. Hydrol.* **604**, 127239.
HAZRA, S.B., GUPTA, A.S. & NIYOGI, P. 1996 On the dispersion of a solute in oscillating flow through a channel. *Heat Mass Transfer* **31** (4), 249–256.
HOLLEY, E.R., HARLEMAN, D.R.F. & FISCHER, H.B. 1970 Dispersion in homogeneous estuary flow. *J. Hydraul. Div.* **96** (8), 1691–1709.
JENSEN, K.H., RIO, E., HANSEN, R., CLANET, C. & BOHR, T. 2009 Osmotically driven pipe flows and their relation to sugar transport in plants. *J. Fluid Mech.* **636**, 371–396.
JIANG, W. & CHEN, G. 2021 Transient dispersion process of active particles. *J. Fluid Mech.* **927**, A11.
JIANG, W., ZENG, L., FU, X. & WU, Z. 2022 Analytical solutions for reactive shear dispersion with boundary adsorption and desorption. *J. Fluid Mech.* **947**, A37.
JIANG, W.Q. & CHEN, G.Q. 2018 Solution of Gill's generalized dispersion model: solute transport in Poiseuille flow with wall absorption. *Intl J. Heat Mass Transfer* **127**, 34–43.
JIANG, Y. & GROTBERG, J.B. 1993 Bolus contaminant dispersion in oscillatory tube flow with conductive walls. *J. Biomech. Engng* **115** (4A), 424–431.
JOSHI, C.H., KAMM, R.D., DRAZEN, J.M. & SLUTSKY, A.S. 1983 An experimental study of gas exchange in laminar oscillatory flow. *J. Fluid Mech.* **133**, 245–254.
KARMAKAR, T., BARIK, S. & RAJA SEKHAR, G.P. 2023 Multi-scale analysis of concentration distribution in unsteady Couette–Poiseuille flows through a porous channel. *Proc. R. Soc. Lond. A* **479** (2269), 20220494.
LAWRENCE, J.J., COENEN, W., SÁNCHEZ, A.L., PAWLAK, G., MARTÍNEZ-BAZÁN, C., HAUGHTON, V. & LASHERAS, J.C. 2019 On the dispersion of a drug delivered intrathecally in the spinal canal. *J. Fluid Mech.* **861**, 679–720.

https://doi.org/10.1017/jfm.2026.11292 Published online by Cambridge University Press

LI, G., WANG, P., JIANG, W.-Q., ZENG, L., LI, Z. & CHEN, G.Q. 2017 Taylor dispersion in wind-driven current. *J. Hydrol.* **555**, 697–707.

MAZUMDER, B.S. & DAS, S.K. 1992 Effect of boundary reaction on solute dispersion in pulsatile flow through a tube. *J. Fluid Mech.* **239**, 523–549.

MEDEROS, G., ARCOS, J., BAUTISTA, O. & MÉNDEZ, F. 2020 Hydrodynamics rheological impact of an oscillatory electroosmotic flow on a mass transfer process in a microcapillary with a reversible wall reaction. *Phys. Fluids* **32** (12), 122003.

MEI, C.C. 1992 Method of homogenization applied to dispersion in porous media. *Transp. Porous Med.* **9** (3), 261–274.

MEI, C.C., AURIAULT, J.-L. & NG, C.-O. 1996 Some applications of the homogenization theory. In *Advances in Applied Mechanics* (ed. J.W. HUTCHINSON & Y. THEODORE), vol. 32, pp. 277–348. Academic Press.

MORRIS, J.F. 2001 Anomalous migration in simulated oscillatory pressure-driven flow of a concentrated suspension. *Phys. Fluids* **13** (9), 2457–2462.

MUKHERJEE, A. & MAZUMDER, B.S. 1988 Dispersion of contaminant in oscillatory flows. *Acta Mechanica* **74** (1–4), 107–122.

NG, C.-O. 2004 A time-varying diffusivity model for shear dispersion in oscillatory channel flow. *Fluid Dyn. Res.* **34** (6), 335–355.

NG, C.-O. 2006 Dispersion in steady and oscillatory flows through a tube with reversible and irreversible wall reactions. *Proc. R. Soc. Lond. A* **462** (2066), 481–515.

NISSAN, A., DROR, I. & BERKOWITZ, B. 2017 Time-dependent velocity-field controls on anomalous chemical transport in porous media. *Water Resour. Res.* **53** (5), 3760–3769.

PAL, P.B., SINGH, S. & MURTHY, P.V.S.N. 2025 Solute dispersion in unsteady and viscous flow regimes of a non-Newtonian fluid flow with periodic body acceleration/deceleration. *Phys. Fluids* **37** (2), 023113.

PAUL, S. & MAZUMDER, B.S. 2008 Dispersion in unsteady Couette–Poiseuille flows. *Intl J. Engng Sci.* **46** (12), 1203–1217.

PAVLIOTIS, G.A. 2002 Homogenization theory for advection–diffusion equations with mean flow. PhD thesis, Rensselaer Polytechnic Institute, Troy.

PAVLIOTIS, G.A. & STUART, A. 2008 *Multiscale Methods: Averaging and Homogenization*. Springer.

PEDLEY, T.J. & KAMM, R.D. 1988 The effect of secondary motion on axial transport in oscillatory tube flow. *J. Fluid Mech.* **193**, 347–367.

PENG, Z. 2024 Macrotransport of active particles in periodic channels and fields: rectification and dispersion. *J. Chem. Phys.* **161** (15), 154101.

PODDAR, N., SAHA, G., MONDAL, K.K., DHAR, S. & MAZUMDER, B.S. 2024 Effect of phase exchange kinetics on Taylor dispersion of chemically reactive solutes in an oscillatory magnetohydrodynamics flow between two parallel plates. *Phys. Fluids* **36** (5), 053601.

RANA, J. & MURTHY, P.V.S.N. 2016 Solute dispersion in pulsatile Casson fluid flow in a tube with wall absorption. *J. Fluid Mech.* **793**, 877–914.

SHAPIRO, M. & BRENNER, H. 1987 Convection and diffusion accompanied by bulk and surface chemical reactions in time-periodic one-dimensional flows. *SIAM J. Appl. Maths* **47** (5), 1061–1075.

SHAPIRO, M. & BRENNER, H. 1990 Taylor dispersion in the presence of time-periodic convection phenomena. Part I. Local-space periodicity. *Phys. Fluids A Fluid Dyn.* **2** (10), 1731–1743.

SINGH, S. & MURTHY, P.V.S.N. 2023 Significance of skewness and kurtosis on the solute dispersion in pulsatile Carreau–Yasuda fluid flow in a tube with wall absorption. *J. Fluid Mech.* **962**, A42.

SMITH, R. 1982*a* Contaminant dispersion in oscillatory flows. *J. Fluid Mech.* **114**, 379–398.

SMITH, R. 1982*b* Dispersion of tracers in the deep ocean. *J. Fluid Mech.* **123**, 131–142.

SMITH, R. 1983 The contraction of contaminant distributions in reversing flows. *J. Fluid Mech.* **129**, 137–151.

SONG, JIE & LAW, A.W.-K. 2015 Longitudinal dispersion of turbulent oscillatory pipe flows. *Environ. Fluid Mech.* **15** (3), 563–593.

TAYLOR, G.I. 1953 Dispersion of soluble matter in solvent flowing slowly through a tube. *Proc. R. Soc. Lond. A* **219** (1137), 186–203.

VEDEL, S. & BRUUS, H. 2012 Transient Taylor–Aris dispersion for time-dependent flows in straight channels. *J. Fluid Mech.* **691**, 95–122.

VEDEL, S., HOVAD, E. & BRUUS, H. 2014 Time-dependent Taylor–Aris dispersion of an initial point concentration. *J. Fluid Mech.* **752**, 107–122.

VEDEL, S., OLESEN, L.H. & BRUUS, H. 2010 Pulsatile microfluidics as an analytical tool for determining the dynamic characteristics of microfluidic systems. *J. Micromech. Microengng* **20** (3), 035026.

WANG, B., JIANG, W., CHEN, G., TAO, L. & LI, Z. 2021 Vertical distribution and longitudinal dispersion of gyrotactic microorganisms in a horizontal plane Poiseuille flow. *Phys. Rev. Fluids* **6** (5), 054502.

https://doi.org/10.1017/jfm.2026.11292 Published online by Cambridge University Press

WANG, B., JIANG, W., ZENG, L., WU, Z. & WANG, P. 2025 Taylor–Aris dispersion of active particles in oscillatory channel flows. *J. Fluid Mech.* **1021**, A3.

WANG, P. & CHEN, G.Q. 2015 Environmental dispersion in a tidal wetland with sorption by vegetation. *Commun. Nonlinear Sci. Numer. Simul.* **22** (1), 348–366.

WANG, P. & CHEN, G.Q. 2017*a* Basic characteristics of Taylor dispersion in a laminar tube flow with wall absorption: exchange rate, advection velocity, dispersivity, skewness and kurtosis in their full time dependance. *Intl J. Heat Mass Transfer* **109**, 844–852.

WANG, P. & CHEN, G.Q. 2017*b* Concentration distribution for pollutant dispersion in a reversal laminar flow. *J. Hydrol.* **551**, 151–161.

WATSON, E.J. 1983 Diffusion in oscillatory pipe flow. *J. Fluid Mech.* **133**, 233–244.

WU, Z. & CHEN, G.Q. 2014 Approach to transverse uniformity of concentration distribution of a solute in a solvent flowing along a straight pipe. *J. Fluid Mech.* **740**, 196–213.

WU, Z., ZENG, L., CHEN, G.Q., LI, Z., SHAO, L., WANG, P. & JIANG, Z. 2012 Environmental dispersion in a tidal flow through a depth-dominated wetland. *Commun. Nonlinear Sci. Numer. Simul.* **17** (12), 5007–5025.

WU, Z., ZHAN, J., ZHU, Z., ZHANG, M., CHANG, L. & FU, X. 2026 Effects of gravitational settling and riverbed-induced mortality on the transport of drifting fish eggs in rivers. *Water Resour. Res.* **62** (1), e2025WR041343.

YANG, Y., JIANG, W.Q., WU, Y.H., WANG, P., WU, Z., ZHANG, B. & ZENG, L. 2021 Migration of buoyancy-controlled active particles in a laminar open-channel flow. *Adv. Water Resour.* **156**, 104023.

YASUDA, H. 1982 Longitudinal dispersion due to the boundary layer in an oscillatory current: theoretical analysis in the case of an instantaneous line source. *J. Oceanogr. Soc. Japan* **38** (6), 385–394.

YASUDA, H. 1984 Longitudinal dispersion of matter due to the shear effect of steady and oscillatory currents. *J. Fluid Mech.* **148**, 383–403.

YOUNG, W.R., RHINES, P.B. & GARRETT, C.J.R. 1982 Shear-flow dispersion, internal waves and horizontal mixing in the ocean. *J. Phys. Oceanogr.* **12** (6), 515–527.

ZENG, H., JIANG, W., GUAN, M., LEE, J.H.-W. & CHEN, G. 2025*a* Dispersion of confined microswimmers with diffuse reflection boundary condition: asymptotic and transient solutions. *J. Fluid Mech.* **1018**, A27.

ZENG, L., CHEN, G.Q., WU, Z., LI, Z., WU, Y.H. & JI, P. 2012 Flow distribution and environmental dispersivity in a tidal wetland channel of rectangular cross-section. *Commun. Nonlinear Sci. Numer. Simul.* **17** (11), 4192–4209.

ZENG, L., YANG, F., WANG, B., JIANG, W., GUAN, M., ZHAO, Y. & WU, Z. 2025b Migration of gyrotactic micro-organisms in surface gravity waves. *Phys. Fluids* **37** (8), 081918.

https://doi.org/10.1017/jfm.2026.11292 Published online by Cambridge University Press